# Dynamics of Decision Making in Animal Group Motion

**Benjamin Nabet · Naomi E. Leonard ·
Iain D. Couzin · Simon A. Levin**

**Abstract**  We analyze a continuous-time model of a multi-agent system motivated by simulation studies on dynamics of decision making in animal groups in motion. Each individual moves at constant speed in the plane and adjusts its heading in response to relative headings of others in the population. The population includes two subgroups that are "informed" such that individuals in each subgroup have a preferred direction of motion. The model exhibits fast and slow time scales allowing for a reduction in

B. Nabet · N.E. Leonard (✉)
Department of Mechanical and Aerospace Engineering, Princeton University, Princeton, NJ 08544,
USA
e-mail: naomi@princeton.edu

B. Nabet
e-mail: bnabet@princeton.edu

I.D. Couzin
Department of Ecology and Evolutionary Biology, Princeton University, Princeton, NJ 08544, USA
e-mail: icouzin@princeton.edu

S.A. Levin
Department of Ecology and Evolutionary Biology, Princeton University, Princeton, NJ 08544, USA
e-mail: slevin@princeton.edu

the dimension of the problem. The stable solutions for the reduced model correspond to compromise by individuals with conflicting preferences. We study the global phase space for the proposed reduced model by computing equilibria and exploring stability and bifurcations.

**Keywords**  Decision making · Dynamical systems · Multi-agent systems · Animal behavior · Collective motion · Coupled oscillators

**Mathematics Subject Classification (2000)**  93A14 · 35B32 · 92D50 · 34C15

## 1 Introduction

Recent research in cooperative control of groups of mobile autonomous agents has led to a growing effort to apply tools from dynamical systems and control theory toward better understanding how biological systems manage collective tasks such as social foraging or migration. In this paper, we derive and study the dynamics of a low-dimensional, minimally parameterized, coordinated control system, motivated by an interest in modeling and predicting the behavior of animal groups in which movement decisions depend in part upon social interactions among group members (Krause and Ruxton 2002; Couzin and Krause 2003; Couzin et al. 2005).

In Couzin et al. (2005), we (IDC and SAL) investigated the mechanisms of decision making and leadership by using a discrete simulation of particles moving in the plane. In this simulation, each particle represents an individual animal and the motion of each individual is influenced by the state of its neighbors (e.g., relative position and relative heading). Within this group, there are two subgroups of informed individuals and one subgroup of naive individuals; each subgroup of informed individuals has a preferred direction of motion (representative of knowledge of the direction to a food source or of a migration route, for example) that it can use to make decisions along with the information on its neighbors. It is shown in (Couzin et al. 2005) that information can be transferred within groups even when there is no signaling, no identification of the informed individuals, and no evaluation of others' information. It was also observed that with two informed subgroups of equal population, the direction of group motion depends on the degree to which the preferred directions differ. For low disagreement, the group follows the average preferred direction of all informed individuals, while for large disagreement the group selects one of the two preferred directions.

Simulations of the sort reported in (Couzin et al. 2005) are highly suggestive, but contain so many degrees of freedom that it becomes difficult to understand the influences of particular mechanisms. To that end, in this paper we seek a lower-dimensional approximation to the individual-based model that will allow deeper investigation of the microscopic reasons for the macroscopic behaviors we observed, and a broader exploration of parameter space. The model we propose and study in a simplified form in this paper is represented by a system of ordinary differential equations. In this formulation, each agent is modeled as a particle moving in the plane at constant speed with steering rate dependent on interparticle measurements and when appropriate on prior information concerning preferred directions. This mathematical framework makes it possible to explore the dynamics in a more general context

and thereby to uncover unifying principles. We show analytically that there are stable motions not observed in the simulation study because relevant initial conditions and/or parameter ranges were not tested. We also explore the nature of instabilities that are not easily understood through simulation. Of more general interest is the insight gained by means of the analysis in this paper toward isolating a biologically plausible mechanism for the decision-making behavior observed in (Couzin et al. 2005) when there are two informed subgroups with conflicting information.

The model in this paper is viewed as an interactive partner to further use of the individual-based simulations, a mutualism that we feel is not sufficiently exploited in the modeling literature. Specifically, the simplifying assumptions we make in this paper yield a model that produces some but not all of the behavior observed in (Couzin et al. 2005), and this deviation focuses attention on a small number of assumptions that may be responsible, including enforcing all-to-all communication, removing a "forgetting factor" feedback term for the informed individuals and ignoring naive individuals. In the next section, we show, for example, that we recover the behavior in (Couzin et al. 2005) when we include only the forgetting factor, a term that allows informed individuals to dynamically devalue their information if they find themselves heading in a very different direction. Driven by the analysis described in this paper, in ongoing work, we are reexamining the simulation to explore the influence of each of these simplifications. An important discovery, to be reported in a future publication, concerns the subtle and nontrivial role of the naive individuals in achieving consensus. These findings complement findings in other contexts, for example, finance (Mauboussin 2006), in which it is increasingly becoming recognized that collective intelligence may be more reliable than what a few leaders provide.

The model presented in this paper is similar to models used for cooperative control of engineered multi-agent systems. For instance, a continuous model of particles moving at constant speed in the plane with steering control (heading rate) designed to couple the dynamics of the particles has been used for stabilization of circular and parallel collective motion (Justh and Krishnaprasad 2004; Sepulchre et al. 2007). The use of the same kinds of models in the engineered and natural settings is no accident. The very efficient and robust ways that animals move together and make collective decisions provide inspiration for design in engineering. Likewise, tools that have been developed for analysis and synthesis in the engineering context may prove useful for investigation in the natural setting. We note that the objectives in engineering applications may be analogous to objectives in the natural setting. For example, in the design of mobile sensor networks (such as the autonomous ocean sampling network described in (Leonard et al. 2007)), the goal is to maximize information intake. This has parallels with optimal social foraging.

The central immediate objective in the present work is to study the global phase space for the proposed simple model by computing equilibria and proving stability and bifurcations. Starting from a large-scale particle model, we reduce it to a simple planar model using a time-scale separation. Fast dynamics are associated with consensus of individuals with similar information and slow dynamics with the subsequent behavior of these different subgroups. In Biyik and Arcak (2006), the authors also use time-scale separation to reduce the dimension of consensus dynamics in complex networks. There the slow and fast times scales are due to sparse and dense connections among nodes in the network.

Our planar particle model includes key features of the discrete-time model of (Couzin et al. 2005), but with important simplifications. For example, we study only the dynamics of the headings, although we define our model for the full spatial dynamics so that positions of agents can also be computed. This specialization is possible because we examine steering laws associated with alignment of individuals and directional preference, consistent with the focus of (Couzin et al. 2005). We prove the validity of a time-scale separation for the model of the heading dynamics of two informed subgroups and one uninformed (naive) subgroup. This time-scale separation was observed in the simulations of (Couzin et al. 2005), even in the case of local sensing. For the bifurcation analysis of the slow dynamics, we focus our study on just two informed subgroups, and motivate the study of the role of uninformed individuals at the end of the paper. We study bifurcations as a function of two bifurcation parameters: $K \geq 0$, the coupling gain that weights the attention paid to neighbors versus the preferred direction, and $\bar{\theta}_2 \in [0, \pi]$, the relative angle of the two preferred directions.

In Sect. 2, we present the model. We identify fast and slow time scales and prove, for the system with two informed subgroups and one naive group, invariance and attractivity of the reduced (slow) manifold. In Sect. 3, we classify the equilibria of the reduced-order system with no naive individuals. In Sect. 4, we prove bifurcations in the system as a function of the coupling gain $K$. In Sects. 5 and 6, we study two specific choices for the parameters $K$ and $\bar{\theta}_2$ for which we can find a closed-form expression for the equilibrium points and compute analytically the bifurcation diagrams. In Sect. 7, we summarize and interpret the results. We explain how the results change for unevenly sized groups of informed individuals. We make final remarks in Sect. 8.

## 2 Models and Time-Scale Separation

### 2.1 Particle Model

We consider a population of $N$ individuals each modeled as a particle moving in the plane. For the purpose of this paper, we assume that every individual can sense every other individual in the population. In the natural setting this all-to-all coupling assumption may be reasonably well justified for tightly clustered groups. Further, as argued in the Introduction, this assumption contributes to our ongoing program to isolate mechanisms and distinguish which are critical to the fundamental behavior observed in (Couzin et al. 2005). In future investigations, we can consider limited sensing and bring to bear the associated theory described in (Sepulchre et al. 2008).

The population is classified into three subgroups. Let $N_1$ and $N_2$ be the number of agents, respectively, in two different subgroups of informed individuals and let $N_3$ be the number of naive (uninformed) individuals such that $N_1 + N_2 + N_3 = N$. Let $\mathcal{N}_1$ and $\mathcal{N}_2$, respectively, be the subsets of indices in $\{1, \dots, N\}$ corresponding to individuals in subgroups 1 and 2, which comprise the two different groups of informed individuals. Let $\mathcal{N}_3$ be the remaining subset of indices corresponding to the naive individuals. Then the cardinality of $\mathcal{N}_k$ is $N_k$, $k = 1, 2, 3$. The preferred heading direction for the individuals in subgroup $i$ is denoted $\bar{\theta}_i$, for $i = 1, 2$.

We model each individual as a particle moving in the plane at constant speed. The heading direction of individual $j$ is denoted $\theta_j$, and $\theta_j$ is allowed to take any value in the circle $S^1$. Let $r_j \in \mathbb{R}^2$ be the position of the $j$th individual moving at constant speed $V_0$, then

$$\dot{r}_j = (V_0 \cos\theta_j, V_0 \sin\theta_j), \quad j = 1, \ldots, N.$$

Our simple model describes the dynamics of the heading angles for all individuals in the population independent of their positions. This model defines steering terms that depend only on relative heading angles. The dynamics are modeled as

$$\dot{\theta}_j = \sin(\bar{\theta}_1 - \theta_j) + \frac{K}{N} \sum_{l=1}^{N} \sin(\theta_l - \theta_j), \quad j \in \mathcal{N}_1,$$

$$\dot{\theta}_j = \sin(\bar{\theta}_2 - \theta_j) + \frac{K}{N} \sum_{l=1}^{N} \sin(\theta_l - \theta_j), \quad j \in \mathcal{N}_2, \tag{1}$$

$$\dot{\theta}_j = \frac{K}{N} \sum_{l=1}^{N} \sin(\theta_l - \theta_j), \quad j \in \mathcal{N}_3.$$

We note that the form of the coupling is based on the Kuramoto model for populations of coupled oscillators (Kuramoto 1984). The model is similar to that used by Mirollo and Strogatz to represent a group of coupled spins in a random magnetic field (Mirollo and Strogatz 1990). In the coupled spin model, there are no subgroups; instead, each individual oscillator has a randomly assigned "pinning" angle $\bar{\theta}_j$ such that the pinning angles are uniformly distributed around the circle. The studied system is known in physics as the mean-field theory for the random-field XY model (Cardy and Ostlund 1982). In (Mirollo and Strogatz 1990), it is proven that the system exhibits a jump bifurcation and hysteresis as $K$ is varied.

## 2.2 Model representation with two time scales

Now let $p_k \in \mathbb{C}$ denote the average of the phasors on the unit circle in the complex plane for the individuals in $\mathcal{N}_k$. In the coupled oscillator literature, $p_k$ is known as the complex order parameter and $\rho_k := |p_k|$ provides a measure of synchrony among the phases. The average phasor $p_k$ is computed as

$$p_k = \rho_k e^{i\Psi_k} = \frac{1}{N_k} \sum_{l \in \mathcal{N}_k} e^{i\theta_l}, \quad k = 1, 2, 3. \tag{2}$$

The parameter $\rho_k$ takes values in the interval $[0, 1]$. It follows that $\rho_k = 1$ if all individuals in $\mathcal{N}_k$ are heading in the same direction (synchronized headings) and $\rho_k = 0$ if individuals in $\mathcal{N}_k$ head in directions such that their averaged velocity is zero. The average direction of individuals in $\mathcal{N}_k$ is $\Psi_k$.

Simulations of the model (1), as shown in Fig. 1, reveal two time scales in the dynamics. First, during a short initial transient time, the heading angles of the individuals in each subgroup synchronize. Then we observe a slow drift until the three average subgroup directions reach the steady state. Motivated by these observations, we
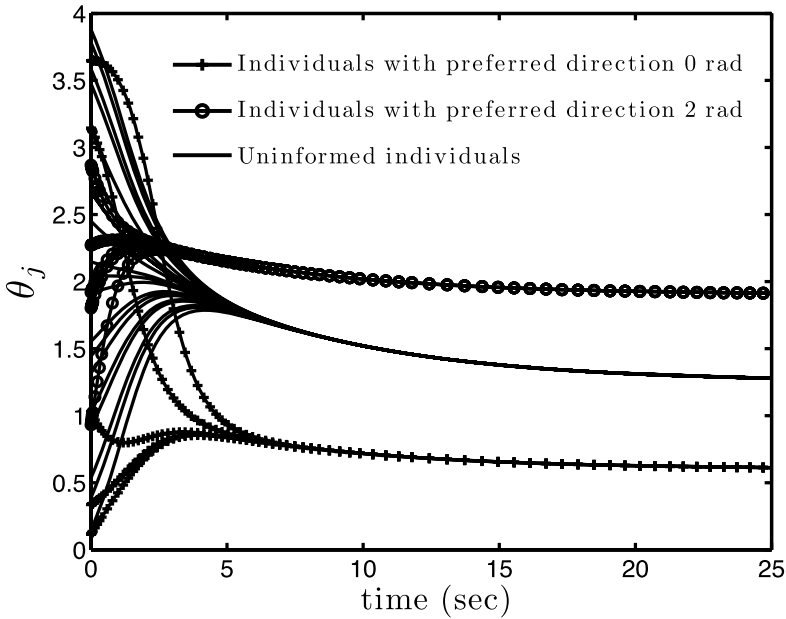
**Fig. 1** Phase angle of each individual in the group versus time for $K = 1$. For this simulation, there are 5 individuals with preferred direction 0 rad, 5 individuals with preferred direction 2 rad, and 20 individuals with no preferred direction. Two time scales in the dynamics can be observed. During a short initial transient time, the heading angles of the individuals in each subgroup synchronize. Then the three average subgroup directions change slowly to their steady state values

define a new set of independent variables that distinguishes slow and fast variables. The average headings $\Psi_1, \Psi_2$, and $\Psi_3$ are the slow variables since they characterize the lumped behavior of each of the three subgroups.

Following (Strogatz 2000),

$$\frac{1}{N} \sum_{l=1}^{N} \sin(\theta_l - \theta_j) = \frac{1}{N} \left( \sum_{k=1}^{3} N_k \rho_k \sin(\Psi_k - \theta_j) \right) \tag{3}$$

and the model (1) becomes

$$\dot{\theta}_j = \sin(\bar{\theta}_1 - \theta_j) + \frac{K}{N} \left( \sum_{k=1}^{3} N_k \rho_k \sin(\Psi_k - \theta_j) \right), \quad j \in \mathcal{N}_1,$$

$$\dot{\theta}_j = \sin(\bar{\theta}_2 - \theta_j) + \frac{K}{N} \left( \sum_{k=1}^{3} N_k \rho_k \sin(\Psi_k - \theta_j) \right), \quad j \in \mathcal{N}_2, \tag{4}$$

$$\dot{\theta}_j = \frac{K}{N} \left( \sum_{k=1}^{3} N_k \rho_k \sin(\Psi_k - \theta_j) \right), \quad j \in \mathcal{N}_3.$$

Summing over each subgroup in (4), we can compute

$$\sum_{j \in \mathcal{N}_1} \dot{\theta}_j = \rho_1 N_1 \sin(\bar{\theta}_1 - \Psi_1) + \frac{K}{N} \rho_1 N_1 \rho_2 N_2 \sin(\Psi_2 - \Psi_1)$$

$$+ \frac{K}{N} \rho_1 N_1 \rho_3 N_3 \sin(\Psi_3 - \Psi_1),$$

$$\sum_{j \in \mathcal{N}_2} \dot{\theta}_j = \rho_2 N_2 \sin(\bar{\theta}_2 - \Psi_2) + \frac{K}{N} \rho_1 N_1 \rho_2 N_2 \sin(\Psi_1 - \Psi_2)$$

$$+ \frac{K}{N} \rho_2 N_2 \rho_3 N_3 \sin(\Psi_3 - \Psi_2),$$

$$\sum_{j \in \mathcal{N}_3} \dot{\theta}_j = \frac{K}{N} \rho_1 N_1 \rho_3 N_3 \sin(\Psi_1 - \Psi_3) + \frac{K}{N} \rho_2 N_2 \rho_3 N_3 \sin(\Psi_2 - \Psi_3).$$

To represent the fast dynamics, we define variables $\alpha_j \in \mathbb{C}$ where

$$\alpha_j = e^{i(N_k \theta_j - \sum_{l \in \mathcal{N}_k} \theta_l)}, \quad j \in \mathcal{N}_k.$$

Then

$$\dot{\alpha}_j = i N_k \alpha_j \left( \dot{\theta}_j - \frac{1}{N_k} \sum_{l \in \mathcal{N}_k} \dot{\theta}_l \right), \quad j \in \mathcal{N}_k.$$

The unit phasors $\alpha_j$ represent how much the heading of individual $j \in \mathcal{N}_k$ differs from $\Psi_k$, the average direction of the subgroup $k$. When all the individuals in the $k$th subgroup have the same heading, $\alpha_j = 1$, $\forall j \in \mathcal{N}_k$. Denote $\boldsymbol{\theta} = (\theta_1, \ldots, \theta_N) \in T^N$ and $\boldsymbol{\alpha}^k = (\alpha_{j_{(k,1)}}, \ldots, \alpha_{j_{(k,N_k-1)}}) \in \mathbb{C}^{N_k-1}$, where $\mathcal{N}_k = \{j_{(k,1)}, \ldots, j_{(k,N_k)}\}$, and consider change of variables $\boldsymbol{\theta} \mapsto \{\boldsymbol{\alpha}^1, \boldsymbol{\alpha}^2, \boldsymbol{\alpha}^3, \Psi_1, \Psi_2, \Psi_3\}$. Further, suppose $K \geq N \gg 1$ and let $\epsilon = 1/K$. By definition, $N_3$ is of the same order or smaller than $N$. We assume that $N_1$ and $N_2$ are such that none of the following are as small as $\epsilon$: $1/N_1$, $1/N_2$, $N_1/N$, $N_2/N$. For example, in case $K = N = 100$, $N_1 = N_2 = 10$, $N_3 = 80$, then $\epsilon = 0.01$ and $1/N_1 = 1/N_2 = N_1/N = N_2/N = 0.1 = \sqrt{\epsilon}$. Given these assumptions, in the new coordinates, the coupled multi-agent system dynamics (1) become

$$\epsilon \dot{\alpha}_j = i N_1 \alpha_j \left( \epsilon \big( \sin(\bar{\theta}_1 - \theta_j) - \rho_1 \sin(\bar{\theta}_1 - \Psi_1) \big) + \frac{N_1}{N} \rho_1 \sin(\Psi_1 - \theta_j) \right.$$

$$\left. + \sum_{k=2,3} \frac{N_k}{N} \rho_k \big( \sin(\Psi_k - \theta_j) - \rho_1 \sin(\Psi_k - \Psi_1) \big) \right)$$

$$=: g_j^1 \big( \boldsymbol{\alpha}^1, \boldsymbol{\alpha}^2, \boldsymbol{\alpha}^3, \Psi_1, \Psi_2, \Psi_3, \epsilon \big), \quad j \in \mathcal{N}_1, \ j \neq j_{(1,N_1)}, \tag{5}$$

$$\epsilon \dot{\alpha}_j = i N_2 \alpha_j \Bigg( \epsilon \big( \sin(\bar{\theta}_2 - \theta_j) - \rho_2 \sin(\bar{\theta}_2 - \Psi_2) \big) + \frac{N_2}{N} \rho_2 \sin(\Psi_2 - \theta_j)$$

$$+ \sum_{k=1,3} \frac{N_k}{N} \rho_k \big( \sin(\Psi_k - \theta_j) - \rho_2 \sin(\Psi_k - \Psi_2) \big) \Bigg)$$

$$=: g_j^2 \big( \boldsymbol{\alpha}^1, \boldsymbol{\alpha}^2, \boldsymbol{\alpha}^3, \Psi_1, \Psi_2, \Psi_3, \epsilon \big), \quad j \in \mathcal{N}_2, \ j \neq j_{(2,N_2)}, \tag{6}$$

$$\epsilon \dot{\alpha}_j = i N_1 \alpha_j \Bigg( \frac{N_3}{N} \rho_3 \sin(\Psi_3 - \theta_j) + \sum_{k=2,3} \frac{N_k}{N} \rho_k \big( \sin(\Psi_k - \theta_j)$$

$$- \rho_3 \sin(\Psi_k - \Psi_3) \big) \Bigg)$$

$$=: g_j^3 \big( \boldsymbol{\alpha}^1, \boldsymbol{\alpha}^2, \boldsymbol{\alpha}^3, \Psi_1, \Psi_2, \Psi_3, \epsilon \big), \quad j \in \mathcal{N}_3, \ j \neq j_{(3,N_3)}, \tag{7}$$

$$\dot{\Psi}_1 = \frac{1}{\rho_1} \sum_{j \in \mathcal{N}_1} \Bigg( \frac{1}{N_1} \sin(\bar{\theta}_1 - \theta_j) + \frac{K}{N} \Bigg( \sum_{k=1}^{3} \frac{N_k}{N_1} \rho_k \sin(\Psi_k - \theta_j) \Bigg) \Bigg) \cos(\Psi_1 - \theta_j)$$

$$=: f_1 \big( \boldsymbol{\alpha}^1, \boldsymbol{\alpha}^2, \boldsymbol{\alpha}^3, \Psi_1, \Psi_2, \Psi_3, \epsilon \big), \tag{8}$$

$$\dot{\Psi}_2 = \frac{1}{\rho_2} \sum_{j \in \mathcal{N}_2} \Bigg( \frac{1}{N_2} \sin(\bar{\theta}_2 - \theta_j) + \frac{K}{N} \Bigg( \sum_{k=1}^{3} \frac{N_k}{N_2} \rho_k \sin(\Psi_k - \theta_j) \Bigg) \Bigg) \cos(\Psi_2 - \theta_j)$$

$$=: f_2 \big( \boldsymbol{\alpha}^1, \boldsymbol{\alpha}^2, \boldsymbol{\alpha}^3, \Psi_1, \Psi_2, \Psi_3, \epsilon \big), \tag{9}$$

$$\dot{\Psi}_3 = \frac{1}{\rho_3} \sum_{j \in \mathcal{N}_3} \Bigg( \frac{K}{N} \Bigg( \sum_{k=1}^{3} \frac{N_k}{N_3} \rho_k \sin(\Psi_k - \theta_j) \Bigg) \Bigg) \cos(\Psi_3 - \theta_j)$$

$$=: f_3 \big( \boldsymbol{\alpha}^1, \boldsymbol{\alpha}^2, \boldsymbol{\alpha}^3, \Psi_1, \Psi_2, \Psi_3, \epsilon \big) \tag{10}$$

for $\rho_k \neq 0$, $k = 1, 2, 3$. In Appendix A, we show that this change of coordinates is well defined.

The models (5)–(10) with $\epsilon \ll 1$ is in the form of a singular perturbation model (Khalil 2002); it exhibits two time scales where the variables $\boldsymbol{\alpha}^1, \boldsymbol{\alpha}^2, \boldsymbol{\alpha}^3$ are the $N - 3$ fast variables and $\Psi_1, \Psi_2, \Psi_3$ are the three slow variables. The solution $\alpha_j = 1$ for $j \in \mathcal{N}_k, k = 1, 2, 3$, equivalently $\theta_j = \Psi_k, j \in \mathcal{N}_k, k = 1, 2, 3$, is an isolated solution of $g_j^k(\boldsymbol{\alpha}^1, \boldsymbol{\alpha}^2, \boldsymbol{\alpha}^3, \Psi_1, \Psi_2, \Psi_3, 0) = 0, k = 1, 2, 3$. For this solution, $\rho_k = 1, k = 1, 2, 3$. In other words, $\theta_j = \Psi_k, j \in \mathcal{N}_k, k = 1, 2, 3$ is an invariant manifold of our system (1). Physically, this means that if we start with all individuals synchronized within their respective subgroup (i.e., $\theta_j = \Psi_k, j \in \mathcal{N}_k, k = 1, 2, 3$), they will stay like this for all time. Let $\mathbf{1} = (1, \ldots, 1)^T$. From the representation of the system dynamics (1) as (5)–(10) with $\epsilon \ll 1$, the corresponding slow dynamics, i.e., dynamics on the invariant manifold are

$$\dot{\Psi}_k = f_k \big( \boldsymbol{\alpha}^1 = \mathbf{1}, \boldsymbol{\alpha}^2 = \mathbf{1}, \boldsymbol{\alpha}^3 = \mathbf{1}, \Psi_1, \Psi_2, \Psi_3, 0 \big), \quad k = 1, 2, 3,$$

which can be written as

$$\dot{\Psi}_1 = \sin(\bar{\theta}_1 - \Psi_1) + \frac{K}{N} N_2 \sin(\Psi_2 - \Psi_1) + \frac{K}{N} N_3 \sin(\Psi_3 - \Psi_1),$$

$$\dot{\Psi}_2 = \sin(\bar{\theta}_2 - \Psi_2) + \frac{K}{N} N_1 \sin(\Psi_1 - \Psi_2) + \frac{K}{N} N_3 \sin(\Psi_3 - \Psi_2), \qquad (11)$$

$$\dot{\Psi}_3 = \frac{K}{N} N_1 \sin(\Psi_1 - \Psi_3) + \frac{K}{N} N_2 \sin(\Psi_2 - \Psi_3).$$

In Appendix B, we prove the reduction by proving the stability of the invariant manifold for the boundary layer dynamics. Singular perturbation theory (see, e.g., Khalil 2002) guarantees then that solutions to the unreduced dynamics stay close to solutions of the reduced system.

Consistent with the observations from simulations in (Couzin et al. 2005), the solution of the fast dynamics corresponds to synchronization of all particle headings in subgroup $k$ to common heading $\Psi_k$, for $k = 1, 2, 3$. The slow dynamics, described by the reduced model (11), dictate the behavior of the common heading $\Psi_k$ of each of the three subgroups, $k = 1, 2, 3$. This reduced model is one in which all the agents in a subgroup (informed subgroups 1 and 2 and naive subgroup 3) behave as a single entity (thus the qualifier "lumped" model) and the intersubgroup coupling term is weighted by the corresponding subgroup population size. This grouping of identical individuals was also observed in the simulation from (Couzin et al. 2005). In that model, the grouping was spatial; each subgroup made a cluster within the group.

In the remaining sections of this paper, we focus our bifurcation analysis on the reduced dynamic model derived here. To further simplify this analysis, we first consider the case that $N_1 = N_2$ and $N_3 = 0$ (i.e., equal population for the two informed subgroups and no naive individuals) and then extend conclusions to the case $N_1 \neq N_2$, $N_3 = 0$ (i.e., when one informed subgroup is more populated than the other and there are still no naive individuals). In the case $N_1 = N_2$ and $N_3 = 0$, (11) becomes

$$\dot{\Psi}_1 = \sin(\bar{\theta}_1 - \Psi_1) + \frac{K}{2} \sin(\Psi_2 - \Psi_1),$$

$$\dot{\Psi}_2 = \sin(\bar{\theta}_2 - \Psi_2) + \frac{K}{2} \sin(\Psi_1 - \Psi_2). \qquad (12)$$

This model also corresponds to the reduced dynamics in the case $N_1 = N_2 \gg 1$ and $K \geq 0$ not necessarily large. Without loss of generality, we set $\bar{\theta}_1 = 0$. The two bifurcation parameters are $K \geq 0$ and $\bar{\theta}_2 \in [0, \pi]$. We note that the general reduced system (11) is a gradient system. In the case of $N_1 = N_2$ and $N_3 = 0$, the dynamics (12) are gradient dynamics such that

$$\dot{\Psi}_k = -\frac{\partial V}{\partial \Psi_k},$$

where $V$ is given by

$$V(\Psi_1, \Psi_2) = -\cos \Psi_1 - \cos(\bar{\theta}_2 - \Psi_2) - \frac{K}{2} \cos(\Psi_2 - \Psi_1).$$

Thus, by LaSalle's invariance principle, all solutions converge to the set of critical points of $V(\Psi_1, \Psi_2)$ and there are no periodic solutions.

Before developing this analysis, we consider an extension of the model (12) where we include a forgetting factor feedback term used in (Couzin et al. 2005) and described in Sect. 1. We compute a corresponding bifurcation plot that exhibits the behavior observed in (Couzin et al. 2005). Although the extended model below is not formally derived by means of the reduction, numerical experiments suggest that it is consistent with the time-scale separation and reflects well the behavior of the unreduced model (1) with the additional forgetting factor feedback. In this extension, the weight an individual places on its preferred direction depends dynamically on how close it is from this preferred direction. When individuals are heading in their preferred direction, the attraction to it is maximal; this influence fades as the heading of an individual moves away from the preferred direction. To introduce this effect in the reduced model, we multiply the "preferred direction" term of (12) by a Gaussian shaped gain as follows:

$$
\begin{aligned}
\dot{\Psi}_1 &= -e^{-\frac{\sin(\Psi_1)^2}{\alpha}} \sin \Psi_1 + \frac{K}{N} \sin(\Psi_2 - \Psi_1), \\
\dot{\Psi}_2 &= e^{-\frac{\sin(\bar{\theta}_2 - \Psi_2)^2}{\alpha}} \sin(\bar{\theta}_2 - \Psi_2) + \frac{K}{N} \sin(\Psi_2 - \Psi_1),
\end{aligned}
\tag{13}
$$

where $\alpha$ is a positive constant chosen to control the width of the Gaussian. The smaller $\alpha$ the quicker an individual gives up on its preferred direction. With this model, for $\bar{\theta}_2$ below a threshold $\bar{\theta}_2^*$, the stable motion corresponds to the two informed groups compromising and splitting the difference in direction of motion. For $\bar{\theta}_2$ above the threshold, the group selects (depending on initial conditions) one of the preferred directions. Figure 2 shows the bifurcation plot for $K = 2.5$ and $\alpha = 0.2$. For $\bar{\theta}_2 < \bar{\theta}_2^*$, the stable motion corresponds to the synchronized motion of both informed subgroups in the average direction, and for $\bar{\theta}_2 > \bar{\theta}_2^*$ there are two stable motions synchronized; one in each of the two preferred directions. There is another bifurcation near $\bar{\theta}_2^*$ when synchronized motion in the direction opposite the average direction becomes stable. The bifurcation plot also illustrates several other unstable solutions, all of these unexplored in the simulation studies of (Couzin et al. 2005).

## 3 Equilibria

The equilibria of system (12) are given by

$$
-\sin \Psi_1 + \frac{K}{2} \sin(\Psi_2 - \Psi_1) = 0,
$$

$$
\sin(\bar{\theta}_2 - \Psi_2) + \frac{K}{2} \sin(\Psi_1 - \Psi_2) = 0.
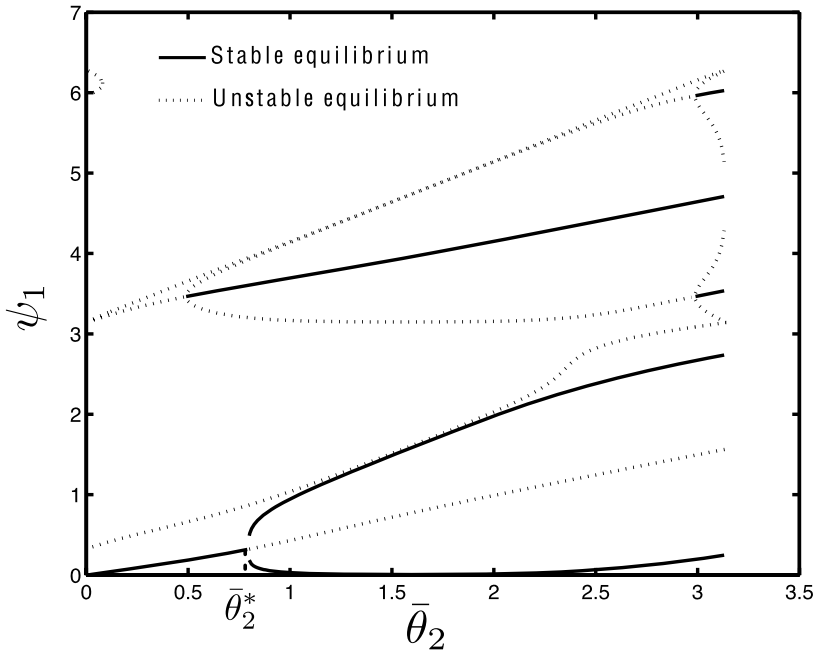$$

**Fig. 2** Bifurcation diagrams for the system (13) with $K = 2.5$, $\alpha = 0.2$. The bifurcation parameter is $\bar{\theta}_2$ and $\Psi_1$ is plotted as a function of $\bar{\theta}_2$ for all equilibria of the system. We observe the supercritical pitchfork bifurcation at $\bar{\theta}_2 = \bar{\theta}_2^*$

There are two sets of solutions, the first set given by

$$\Psi_1 = \pi - \bar{\theta}_2 + \Psi_2,$$
$$\sin(\Psi_2 - \bar{\theta}_2) = \frac{K}{2} \sin \bar{\theta}_2, \tag{14}$$

and the second set given by

$$\Psi_1 = \bar{\theta}_2 - \Psi_2, \tag{15}$$

$$\sin(\bar{\theta}_2 - \Psi_2) = \frac{K}{2} \sin(2\Psi_2 - \bar{\theta}_2). \tag{16}$$

*First Set of Solutions* Equation (14) has two solutions: $\Psi_2 = \bar{\theta}_2 + \arcsin(\frac{K}{2} \sin \bar{\theta}_2)$ and $\Psi_2 = \pi + \bar{\theta}_2 - \arcsin(\frac{K}{2} \sin \bar{\theta}_2)$. These two solutions exist if and only if $|\frac{K}{2} \sin \bar{\theta}_2| \leq 1$.

**Lemma 3.1** *If $|\frac{K}{2} \sin \bar{\theta}_2| < 1$, the two equilibria $\boldsymbol{\psi}_{S1} = (\Psi_1, \Psi_2)_{S1}$ and $\boldsymbol{\psi}_{S2} = (\Psi_1, \Psi_2)_{S2}$ satisfying (14) given by*

$$\boldsymbol{\psi}_{S1} = \left( \pi + \arcsin\left( \frac{K}{2} \sin \bar{\theta}_2 \right), \bar{\theta}_2 + \arcsin\left( \frac{K}{2} \sin \bar{\theta}_2 \right) \right), \tag{17}$$

$$\boldsymbol{\psi}_{S2} = \left( -\arcsin\left(\frac{K}{2}\sin\bar{\theta}_2\right), \pi + \bar{\theta}_2 - \arcsin\left(\frac{K}{2}\sin\bar{\theta}_2\right) \right), \qquad (18)$$

*are saddle points* $\forall K > 0$ *and* $\forall \bar{\theta}_2 \in [0, \pi]$. *If* $\frac{K}{2}\sin\bar{\theta}_2 = 1$, *then* $\boldsymbol{\psi}_{S1} = \boldsymbol{\psi}_{S2}$. *In this case, if also* $K > 0$ *and* $\bar{\theta}_2 \in (0, \frac{\pi}{2}) \cup (\frac{\pi}{2}, \pi)$ *then* $\boldsymbol{\psi}_{S1} = \boldsymbol{\psi}_{S2}$ *is unstable with one zero eigenvalue and one positive real eigenvalue. If* $\bar{\theta}_2 = \frac{\pi}{2}$ *(and* $K = 2$*) then both eigenvalues are zero.*

*Proof* The linearization of (12) at each of the two equilibria $\boldsymbol{\psi}_{S1}$ or $\boldsymbol{\psi}_{S2}$ gives the same symmetric Jacobian with eigenvalues $\lambda_1, \lambda_2 \in \mathbb{R}$ satisfying

$$\lambda_1 \lambda_2 = \frac{K^2}{4}\sin^2\bar{\theta}_2 - 1 < 0 \quad \text{for } \left|\frac{K}{2}\sin\bar{\theta}_2\right| < 1.$$

For $\bar{\theta}_2 \in [0, \pi]$, the eigenvalues are of opposite sign. This implies that $\boldsymbol{\psi}_{S1}$ and $\boldsymbol{\psi}_{S2}$ are saddle points $\forall K > 0$ and $\forall\bar{\theta}_2 \in [0, \pi]$ if $\frac{K}{2}\sin\bar{\theta}_2 < 1$. In the case $|\frac{K}{2}\sin\bar{\theta}_2| = 1$, $\boldsymbol{\psi}_{S1} = \boldsymbol{\psi}_{S2} = (\frac{3\pi}{2}, \frac{\pi}{2} + \bar{\theta}_2)$ and the eigenvalues are $\lambda_1 = 0$ and $\lambda_2 = K\cos\bar{\theta}_2 > 0$. Therefore, for $\bar{\theta}_2 \in (0, \frac{\pi}{2}) \cup (\frac{\pi}{2}, \pi)$, the equilibria $\boldsymbol{\psi}_{S1} = \boldsymbol{\psi}_{S2} = (\frac{3\pi}{2}, \frac{\pi}{2} + \bar{\theta}_2)$ are unstable with one zero eigenvalue and one strictly positive eigenvalue. In case $\bar{\theta}_2 = \pi/2$ and $K = 2$, $\lambda_1 = \lambda_2 = 0$.                                                            $\square$

The case in which $\bar{\theta}_2 = \frac{\pi}{2}$ is studied further in Sect. 4.2.

*Second Set of Solutions*    In order to study (15)–(16), we make a change of variables $(\Psi_1, \Psi_2) \mapsto (\rho, \Psi)$ where $\rho \in [0, 1]$ and $\Psi \in S^1$ are defined by

$$\rho e^{i\Psi} = \frac{1}{2}\left(e^{i\Psi_1} + e^{i\Psi_2}\right) = \cos\left(\frac{\Psi_1 - \Psi_2}{2}\right)e^{i(\Psi_1 + \Psi_2)/2} \qquad (19)$$

$$= \cos\left(\frac{\bar{\theta}_2}{2} - \Psi_2\right)\left(\cos\frac{\bar{\theta}_2}{2} + i\sin\frac{\bar{\theta}_2}{2}\right) \qquad (20)$$

and (20) follows from (15). For $\bar{\theta}_2 \in [0, \pi]$, (15) then implies that $\Psi = \frac{\bar{\theta}_2}{2}$ or $\Psi = \frac{\bar{\theta}_2}{2} + \pi$. We can rewrite (16) as

$$\sin\frac{\bar{\theta}_2}{2}\cos\left(\frac{\bar{\theta}_2}{2} - \Psi_2\right) + \cos\frac{\bar{\theta}_2}{2}\sin\left(\frac{\bar{\theta}_2}{2} - \Psi_2\right)$$

$$+ K\sin\left(\frac{\bar{\theta}_2}{2} - \Psi_2\right)\cos\left(\frac{\bar{\theta}_2}{2} - \Psi_2\right) = 0. \qquad (21)$$

In Sect. 6, we study the special case $\bar{\theta}_2 = \pi$. Here, we focus on $\bar{\theta}_2 \in [0, \pi)$.

For $\Psi = \frac{\bar{\theta}_2}{2}$, (20) implies that $\cos(\frac{\bar{\theta}_2}{2} - \Psi_2) = \rho$ and $\sin(\frac{\bar{\theta}_2}{2} - \Psi_2) = \pm\sqrt{1 - \rho^2}$. Accordingly, (21) implies that $\rho$ satisfies

$$\rho\sin\frac{\bar{\theta}_2}{2} + \sqrt{1 - \rho^2}\cos\frac{\bar{\theta}_2}{2} + K\rho\sqrt{1 - \rho^2} = 0 \qquad (22)$$

or

$$\rho \sin \frac{\bar{\theta}_2}{2} - \sqrt{1 - \rho^2} \cos \frac{\bar{\theta}_2}{2} - K\rho\sqrt{1 - \rho^2} = 0. \tag{23}$$

These imply that $\rho = 1$ if and only if $\bar{\theta}_2 = 0$, and $\rho = 0$ if and only if $\bar{\theta}_2 = \pi$. For $\bar{\theta}_2 \in (0, \pi)$, (22) does not have any solution for $\rho \in (0, 1)$ since every term on the left is positive, and (23) has one solution for $\rho \in (0, 1)$. We call the corresponding equilibrium $\boldsymbol{\psi}_{\text{sync1}} := (\Psi_1, \Psi_2)_{\text{sync1}}$. In the case $\bar{\theta}_2 = 0$, $\boldsymbol{\psi}_{\text{sync1}} = (0, 0)$.

**Lemma 3.2** *The equilibrium $\boldsymbol{\psi}_{\text{sync1}}$ is a stable node for all $(K, \bar{\theta}_2) \in [0, \infty) \times [0, \pi)$.*

*Proof* Using $\cos(\frac{\bar{\theta}_2}{2} - \Psi_2) = \rho$ and $\sin(\frac{\bar{\theta}_2}{2} - \Psi_2) = -\sqrt{1 - \rho^2}$, the Jacobian at the equilibrium is computed; it is symmetric and the corresponding eigenvalues are

$$\lambda_{1,2} = -\left(\rho \cos \frac{\bar{\theta}_2}{2} + \sqrt{1 - \rho^2} \sin \frac{\bar{\theta}_2}{2} + \frac{K}{2}(2\rho^2 - 1)\right) \pm \frac{K}{2}(2\rho^2 - 1).$$

We find using (23) for all $(K, \bar{\theta}_2) \in [0, \infty) \times [0, \pi)$ that

$$-\sqrt{1 - \rho^2} \sin \frac{\bar{\theta}_2}{2} - K(2\rho^2 - 1) = -\frac{1}{\rho}(1 - \rho^2) \cos \frac{\bar{\theta}_2}{2} - K\rho^2 < 0. \tag{24}$$

Thus, for all $(K, \bar{\theta}_2) \in [0, \infty) \times [0, \pi)$, using (24) both eigenvalues are real and negative. Hence, $\boldsymbol{\psi}_{\text{sync1}}$ is a stable node for all $(K, \bar{\theta}_2) \in [0, \infty) \times [0, \pi)$. $\qquad\square$

For $\Psi = \frac{\bar{\theta}_2}{2} + \pi$, (20) implies that $\cos(\frac{\bar{\theta}_2}{2} - \Psi_2) = -\rho$ and $\sin(\frac{\bar{\theta}_2}{2} - \Psi_2) = \pm\sqrt{1 - \rho^2}$. Hence, by (21) $\rho$ has to satisfy

$$-\rho \sin \frac{\bar{\theta}_2}{2} + \sqrt{1 - \rho^2} \cos \frac{\bar{\theta}_2}{2} - K\rho\sqrt{1 - \rho^2} = 0 \tag{25}$$

or

$$-\rho \sin \frac{\bar{\theta}_2}{2} - \sqrt{1 - \rho^2} \cos \frac{\bar{\theta}_2}{2} + K\rho\sqrt{1 - \rho^2} = 0. \tag{26}$$

Equation (25) has one solution for $\rho \in [0, 1]$; we call the corresponding equilibrium $\boldsymbol{\psi}_{\text{antisync1}} := (\Psi_1, \Psi_2)_{\text{antisync1}}$.

**Lemma 3.3** *The equilibrium $\boldsymbol{\psi}_{\text{antisync1}}$ is unstable for all $(K, \bar{\theta}_2) \in [0, \infty) \times [0, \pi)$.*

*Proof* Using $\cos(\frac{\bar{\theta}_2}{2} - \Psi_2) = -\rho$ and $\sin(\frac{\bar{\theta}_2}{2} - \Psi_2) = \sqrt{1 - \rho^2}$, the Jacobian evaluated at this equilibrium has eigenvalues

$$\lambda_{1,2} = \rho \cos \frac{\bar{\theta}_2}{2} + \sqrt{1 - \rho^2} \sin \frac{\bar{\theta}_2}{2} - \frac{K}{2}(2\rho^2 - 1) \pm \frac{K}{2}(2\rho^2 - 1).$$

One eigenvalue is equal to $\rho \cos \frac{\bar{\theta}_2}{2} + \sqrt{1-\rho^2} \sin \frac{\bar{\theta}_2}{2} > 0$ for all $(K, \bar{\theta}_2) \in [0, \infty) \times [0, \pi)$. Hence, $\boldsymbol{\psi}_{\text{antisync1}}$ is unstable for all $(K, \bar{\theta}_2) \in [0, \infty) \times [0, \pi)$. $\qquad\square$

Equation (26) has between zero and two solutions for $\rho \in [0, 1]$. The equilibria we get from (26) when they exist are called $\boldsymbol{\psi}_{\text{sync2}} := (\Psi_1, \Psi_2)_{\text{sync2}}$ and $\boldsymbol{\psi}_{\text{antisync2}} := (\Psi_1, \Psi_2)_{\text{antisync2}}$.

**Lemma 3.4** *Equation* (26) *has two solutions* $(\rho_{\text{antisync2}}, \rho_{\text{sync2}})$ *when* $K > K_1$,

$$K_1 = \left( \cos\left(\frac{\bar{\theta}_2}{2}\right)^{\frac{2}{3}} + \sin\left(\frac{\bar{\theta}_2}{2}\right)^{\frac{2}{3}} \right)^{\frac{3}{2}},$$

*such that*

$$0 < \rho_{\text{antisync2}} < \sqrt{1 - \left( \frac{\sin \frac{\bar{\theta}_2}{2}}{K} \right)^{\frac{2}{3}}} < \rho_{\text{sync2}} < \sqrt{1 - \left( \frac{\sin \frac{\bar{\theta}_2}{2}}{K} \right)^2} < 1. \quad (27)$$

*Proof* We define $K' = \frac{K}{\sin \frac{\bar{\theta}_2}{2}}$, which is valid except for the trivial case when $\bar{\theta}_2 = 0$. Equation (26) becomes

$$g(\rho) := \rho \left( \frac{1}{\sqrt{1-\rho^2}} - K' \right) = -\cot \frac{\bar{\theta}_2}{2}. \quad (28)$$

The solutions of (26) exist when the function $g(\rho)$ intersects the constant $y = -\cot \frac{\bar{\theta}_2}{2} < 0$. The function $g(\rho)$ goes to zero when $\rho \to 0$, and to $+\infty$ when $\rho \to 1$ reaching its minimum of $-K'(\rho^*)^3$ at $\rho^* = \sqrt{1 - \frac{1}{K'^{2/3}}}$. Equation (26) will have two solutions $(\rho_1, \rho_2)$ flanking $\rho^*$ if and only if $g(\rho^*) < -\cot \frac{\bar{\theta}_2}{2}$, which is satisfied if and only if

$$K > K_1 = \left( \cos\left(\frac{\bar{\theta}_2}{2}\right)^{\frac{2}{3}} + \sin\left(\frac{\bar{\theta}_2}{2}\right)^{\frac{2}{3}} \right)^{\frac{3}{2}}. \quad (29)$$

The two solutions $(\rho_{\text{antisync2}}, \rho_{\text{sync2}})$ have to be smaller than the zero of the function $g(\rho)$ given by

$$\sqrt{1 - \left( \frac{\sin \frac{\bar{\theta}_2}{2}}{K} \right)^2} < 1,$$

which concludes the proof. We note that given the form of $g(\rho)$, $\rho_{\text{antisync2}}$ ($\rho_{\text{sync2}}$) is a decreasing (increasing) function of $K$. $\qquad\square$

We now present stability results for these equilibria.

**Lemma 3.5** *The equilibrium* $\boldsymbol{\psi}_{\text{sync2}}$ *is unstable for all* $(K, \bar{\theta}_2) \in [K_1, \infty) \times [0, \frac{\pi}{2}) \cup [K_0, \infty) \times (\frac{\pi}{2}, \pi)$ *and stable for all* $(K, \bar{\theta}_2) \in [K_1, K_0) \times (\frac{\pi}{2}, \pi)$, *where* $K_1 < K_0 = \frac{2}{\sin \bar{\theta}_2}$.

*Proof* We prove these results by looking at the eigenvalues of the Jacobian. We first consider the case when $\bar{\theta}_2 < \frac{\pi}{2}$ and $K > K_1$ and show that one eigenvalue is real and positive. The eigenvalues of the Jacobian are given by

$$\lambda_{1,2} = \rho \cos \frac{\bar{\theta}_2}{2} - \sqrt{1 - \rho^2} \sin \frac{\bar{\theta}_2}{2} - \frac{K}{2}(2\rho^2 - 1) \pm \frac{K}{2}(2\rho^2 - 1). \tag{30}$$

For all $K > K_1$, the inequalities in (27) yield

$$\lambda_1 > \sqrt{\frac{1}{1 + \tan(\frac{\bar{\theta}_2}{2})^{\frac{2}{3}}}} \cos \frac{\bar{\theta}_2}{2} - \sqrt{\frac{1}{1 + \cot(\frac{\bar{\theta}_2}{2})^{\frac{2}{3}}}} \sin \frac{\bar{\theta}_2}{2} > 0 \quad \text{if } \bar{\theta}_2 < \frac{\pi}{2}, \tag{31}$$

proving that for $(K, \bar{\theta}_2) \in [K_1, \infty) \times [0, \frac{\pi}{2})$ the equilibrium $\boldsymbol{\psi}_{\text{sync2}}$ is unstable.

We now consider the case when $\bar{\theta}_2 > \frac{\pi}{2}$ and show that for $K \in (K_1, K_0)$, both eigenvalues $\lambda_1, \lambda_2$ are negative and that for $K > K_0 \; \lambda_1 > 0$. When $K = K_1$, (26) has one solution in [0, 1], namely

$$\rho_1 = \sqrt{\frac{\cos(\frac{\bar{\theta}_2}{2})^{\frac{2}{3}}}{\cos(\frac{\bar{\theta}_2}{2})^{\frac{2}{3}} + \sin(\frac{\bar{\theta}_2}{2})^{\frac{2}{3}}}}.$$

The eigenvalues $\lambda_1$ and $\lambda_2$ evaluated at $K = K_1$, $\rho = \rho_1$ are given by

$$\lambda_1|_{K_1, \rho_1} = \sqrt{\frac{1}{1 + \tan(\frac{\bar{\theta}_2}{2})^{\frac{2}{3}}}} \cos \frac{\bar{\theta}_2}{2} - \sin \frac{\bar{\theta}_2}{2} \sqrt{\frac{1}{1 + \cot(\frac{\bar{\theta}_2}{2})^{\frac{2}{3}}}} < 0 \quad \text{if } \bar{\theta}_2 > \frac{\pi}{2},$$

$$\lambda_2|_{K_1, \rho_1} = 0.$$

The derivatives of $\lambda_1$ and $\lambda_2$ with respect to $K$ are given by

$$\frac{\partial \lambda_1}{\partial K} = \left( \cos \frac{\bar{\theta}_2}{2} + \frac{\rho}{\sqrt{1 - \rho^2}} \sin \frac{\bar{\theta}_2}{2} \right) \frac{\partial \rho}{\partial K},$$

$$\frac{\partial \lambda_2}{\partial K} = \left( \cos \frac{\bar{\theta}_2}{2} + \frac{\rho}{\sqrt{1 - \rho^2}} \sin \frac{\bar{\theta}_2}{2} - 4K\rho \right) \frac{\partial \rho}{\partial K} - (2\rho^2 - 1). \tag{32}$$

As we noted in the proof of Lemma 3.4, $\rho_{\text{sync2}}$ is an increasing function of $K$, implying that $\frac{\partial \rho}{\partial K}|_{\psi_{\text{sync2}}} > 0$. Using, in addition, the inequalities (27) we get for $\bar{\theta}_2 > \frac{\pi}{2}$ that

$$\left. \frac{\partial \lambda_1}{\partial K} \right|_{\psi_{\text{sync2}}} > 0, \tag{33}$$

$$\left.\frac{\partial \lambda_2}{\partial K}\right|_{\Psi_{\text{sync2}}} < -2\cos\frac{\bar{\theta}_2}{2} - 3\cos\left(\frac{\bar{\theta}_2}{2}\right)^{\frac{1}{3}}\sin\left(\frac{\bar{\theta}_2}{2}\right)^{\frac{2}{3}} + \frac{\sin(\frac{\bar{\theta}_2}{2})^{\frac{2}{3}} - \cos(\frac{\bar{\theta}_2}{2})^{\frac{2}{3}}}{\sin(\frac{\bar{\theta}_2}{2})^{\frac{2}{3}} + \cos(\frac{\bar{\theta}_2}{2})^{\frac{2}{3}}} < 0. \tag{34}$$

Equation (34) implies that $\lambda_2|_{\Psi_{\text{sync2}}} < 0$, $\forall K > K_1$. Equation (33) implies that $\lambda_1|_{\Psi_{\text{sync2}}}$ is a strictly increasing function of $K$. Since $\lambda_1|_{K_1,\rho_1} < 0$, $\lambda_1|_{\Psi_{\text{sync2}}}$ will cross zero exactly once. When $K = K_0$, the solution of (26) is $\rho_0 = \sin\frac{\bar{\theta}_2}{2}$ and so $\lambda_1|_{K_0,\rho_0} = 0$. Thus, $\lambda_1$ will be negative for $K < K_0$ and positive for $K > K_0$. □

**Lemma 3.6** *The equilibrium* $\boldsymbol{\psi}_{\text{antisync2}}$ *is unstable for all* $(K, \bar{\theta}_2) \in [K_1, \infty) \times [0, \pi)$.

*Proof* We prove this lemma by showing that $\lambda_2|_{\boldsymbol{\psi}_{\text{antisync2}}} > 0$. Since on the branch of equilibria $\boldsymbol{\psi}_{\text{antisync2}}$, (26) is satisfied, taking partial derivative of both sides of (26) with respect to $K$ and using the expression for $\lambda_2$ (30) yields

$$\frac{\partial \rho}{\partial K} = \frac{\rho(\rho^2 - 1)}{\lambda_2}. \tag{35}$$

Plugging (35) into (32), we get

$$\frac{\partial \lambda_2}{\partial K} = \frac{-\rho^3 \cos\frac{\bar{\theta}_2}{2} + K - (1 - \rho^2)^{\frac{3}{2}}\sin\frac{\bar{\theta}_2}{2}}{\lambda_2}. \tag{36}$$

For all $K > K_1$, $\rho \in [0, 1]$, the numerator of (36) is strictly positive. This implies that $\lambda_2$ does not change sign as a function of $K$. At $K = K_1$, $\lambda_2 = 0$. We check that on the branch of $\boldsymbol{\psi}_{\text{antisync2}}$, when $K = 2$, $\lambda_2 = \cos\bar{\theta}_2 > 0$ implying that for all $K > K_1$, $\lambda_2|_{\boldsymbol{\psi}_{\text{antisync2}}} > 0$. □

For all solutions (of the second set), in (23), (25), and (26), as $K$ gets increasingly large, $K\rho\sqrt{1 - \rho^2}$ must approach zero. This means that as $K \to \infty$ then $\rho \to 0$ or $\rho \to 1$. We call an equilibrium *synchronized* if $\Psi_1 = \Psi_2 \bmod 2\pi$ and *antisynchronized* if $\Psi_1 - \Psi_2 = \pi \bmod 2\pi$. Thus, for very large values of $K$, all the equilibria will be either *synchronized* ($\rho \to 1$) or *anti-synchronized* ($\rho \to 0$). For modest values of $K$, the strength of the coupling is less than or equal to the strength of the attraction to the preferred direction, and the equilibria are typically neither fully synchronized nor fully antisynchronized. In this case, we call an equilibrium *K-almost synchronized* (*K-almost antisynchronized*) if the corresponding equilibrium in the case $K \gg 1$, is synchronized (antisynchronized). Thus, $K$-almost synchronization occurs at $\Psi = \frac{\bar{\theta}_2}{2}$ and $\Psi = \frac{\bar{\theta}_2}{2} + \pi$. Note that these solutions correspond to an exact compromise between the two preferred directions.

Figure 3 shows two bifurcation diagrams in the cases (a) $\bar{\theta}_2 = 1$ rad and (b) $\bar{\theta}_2 = 2$ rad with bifurcation parameter $K$. The synchrony measure $\rho$, as defined by (19), is plotted as a function of $K$ for all equilibria in the second set of solutions. There are two equilibria that do not exist for low enough values of $K$; these two equilibria are the solution from (26). We also note in comparing Figs. 3(a) and (b) that the stability of these two equilibria changes as a function of $K$ and $\bar{\theta}_2$, indicating the presence
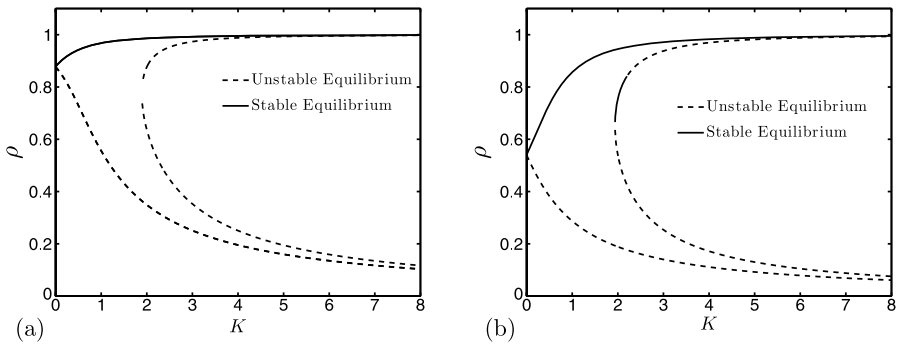
**Fig. 3** Bifurcation diagrams in cases (**a**) $\bar{\theta}_2 = 1$ rad and (**b**) $\bar{\theta}_2 = 2$ rad. The bifurcation parameter is $K$ and $\rho$ is plotted as a function of $K$ for all equilibria in the second set of solutions. We note that two equilibria do not exist for low values of $K$. Stability of these same two equilibria changes type between (**a**) and (**b**), indicating the presence of bifurcations

of bifurcations. The other two equilibria can be seen to be defined for all values of $K$. The stable node is $\boldsymbol{\psi}_{\text{sync1}}$ which is the solution to (23). This equilibrium becomes synchronized as $K$ increases, i.e., $\rho \to 1$ as $K \to \infty$. The unstable node is $\boldsymbol{\psi}_{\text{antisync1}}$ which comes from (25). This equilibrium becomes antisynchronized as $K$ increases, i.e., $\rho \to 0$ as $K \to \infty$. As predicted above, it can be seen that as $K$ increases $\rho$ approaches 0 or 1 also for the two other equilibria.

## 4 Bifurcations in the $(K, \boldsymbol{\Psi}_i)$ Plane

As we observed in Sect. 3, the system (12) undergoes bifurcations as we vary the two bifurcation parameters $K$ and $\bar{\theta}_2$. For example, the two equilibria given by the first set of solutions, $\boldsymbol{\psi}_{S1}$ and $\boldsymbol{\psi}_{S2}$, are defined if and only if $\frac{K}{2}\sin\bar{\theta}_2 \leq 1$. Also, we recall that the equilibria given by (26) are not always defined and their stability type is dependent on the values of $K$ and $\bar{\theta}_2$. In Sect. 5, we study the analytically solvable case $K = 2$. The case $\bar{\theta}_2 = \pi$, also solvable analytically, is treated in Sect. 6. In this section, we consider bifurcations in $K$ for $\bar{\theta}_2$ taking fixed value in three different intervals; first for $\frac{\pi}{2} < \bar{\theta}_2 < \pi$, then for $\bar{\theta}_2 = \frac{\pi}{2}$, and finally for $0 < \bar{\theta}_2 < \frac{\pi}{2}$. Figure 4 shows bifurcation diagrams with $\bar{\theta}_2$ fixed in each of these three intervals. The angle $\Psi_1$ is plotted as a function of bifurcation parameter $K$. These plots are computed by solving numerically for the equilibria and characterizing the stability by computing the eigenvalues of the Jacobian.

### 4.1 Bifurcations in the $(K, \Psi_i)$ Plane for $\frac{\pi}{2} < \bar{\theta}_2 < \pi$

The bifurcation diagram in the $(K, \Psi_i)$ plane for $\bar{\theta}_2 = \frac{3\pi}{4}$ is plotted in Fig. 4(a). This is representative of the case $\frac{\pi}{2} < \bar{\theta}_2 < \pi$. There are two bifurcations: one at $K = K_1$ when two equilibria appear and one at $K = K_0 > K_1$ when two equilibria disappear. For $K_1 < K < K_0$, there are two stable equilibria whereas there is only one stable equilibrium when $K$ is outside this region. The one stable equilibrium
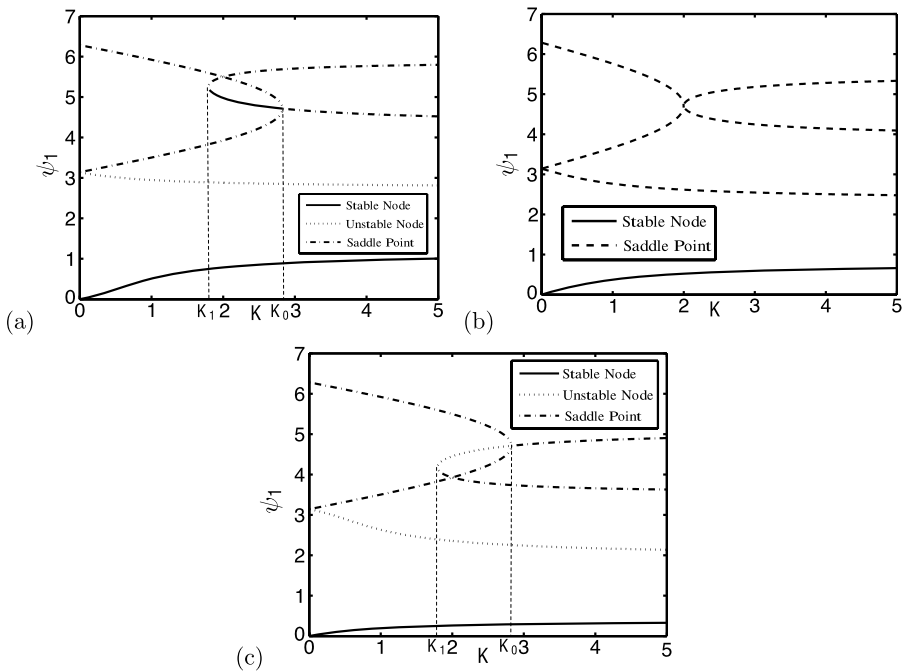
**Fig. 4** Bifurcation diagrams in cases (**a**) $\bar{\theta}_2 = \frac{3\pi}{4}$, (**b**) $\bar{\theta}_2 = \frac{\pi}{2}$, and (**c**) $\bar{\theta}_2 = \frac{\pi}{4}$. The bifurcation parameter is $K$ and $\Psi_1$ is plotted as a function of $K$ for all equilibria of the system. We observe the hypercritical pitchfork bifurcation for $\bar{\theta}_2 = \frac{3\pi}{4}$ at $K = K_0$. For the case $\bar{\theta}_2 = \frac{\pi}{4}$, the bifurcation at $K = K_0$ only consists of a change in the number of equilibria, but does not affect the stability of the system. In the case that $\bar{\theta}_2 = \frac{\pi}{2}$, the bifurcation only consists in the disappearance of two saddle points simultaneously with the appearance of two new ones

that exists for all $K \geq 0$ is $\boldsymbol{\psi}_{\text{sync1}}$. The second stable equilibrium appears through a saddle node bifurcation. We can (partially) prove that the second stable equilibrium disappears through a hypercritical pitchfork at $K = K_0$. From Lemma 3.1, when $K = K_0 = 2/\sin\bar{\theta}_2$, the two equilibria $\boldsymbol{\psi}_{S1}$ and $\boldsymbol{\psi}_{S2}$ meet and are equal to $\boldsymbol{\psi}_0 = (\Psi_1, \Psi_2)_0 = (\frac{3\pi}{2}, \bar{\theta}_2 + \frac{\pi}{2})$. For $K > K_0$, $\boldsymbol{\psi}_{S1}$ and $\boldsymbol{\psi}_{S2}$ no longer exist. With the change of variable $(\Psi_1, \Psi_2) \mapsto (\rho, \Psi)$ defined by (19) where $\rho \in [0, 1]$ and $\Psi \in S^1$, the equilibrium $\boldsymbol{\psi}_{S1} = \boldsymbol{\psi}_{S2} = \boldsymbol{\psi}_0$ for $K = K_0$ becomes $(\rho, \Psi)_0 = (\sin\frac{\bar{\theta}_2}{2}, \frac{\bar{\theta}_2}{2} + \pi)$. This equilibrium also solves (26) and corresponds to $\boldsymbol{\psi}_{\text{sync2}}$ at $K = K_0$. Hence, a third branch of equilibria from the second set of solutions goes through the bifurcation point $K = K_0$. It is easy to show that no other branch of equilibria crosses.

In order to prove that the bifurcation $K = K_0$ is a *hypercritical pitchfork bifurcation*, we use the extension for pitchforks of the general theorem for saddle node bifurcations in (Guckenheimer and Holmes 1983). However, of the three conditions to check in the theorem, we can verify only the first two. Thus, this is a partial proof.

1. *Nondegeneracy of the linearization.*

   The linearization of (12) at $\boldsymbol{\psi} = \boldsymbol{\psi}_0$ and $K = K_0$ is easily checked to be non-degenerate since the Jacobian has a simple zero eigenvalue.

2. *Transversality condition to control nondegeneracy with respect to the parameter.*
    To check this, we show that the equilibrium $\psi_{\text{sync2}}$ goes from stable to unstable through the bifurcation. This follows from the proof of Lemma 3.5, since $\lambda_1|_{\psi_{\text{sync2}}}$ is negative for $K < K_0$ and positive for $K > K_0$ and $\lambda_2|_{\psi_{\text{sync2}}}$ is negative for $K > K_0 > K_1$.

3. *Transversality condition to control nondegeneracy with respect to the dominant effect of the cubic nonlinear term.*
    A straightforward computation is inconclusive. Instead, to prove the condition, we suggest to show that the dynamics on the center manifold have a nondegenerate cubic term. If this can successfully be carried out, we expect the sign of the cubic term to be positive proving that the bifurcation is a hypercritical pitchfork.

### 4.2 Bifurcations in the $(K, \Psi_i)$ Plane for $\bar{\theta}_2 = \frac{\pi}{2}$

The bifurcation diagram in the $(K, \Psi_i)$ plane for $\bar{\theta}_2 = \frac{\pi}{2}$ is plotted in Fig. 4(b). There is one bifurcation at $K = 2$ when two equilibria disappear and two new ones appear. From Sect. 3, we observe that there is a bifurcation at $\frac{K}{2} \sin \bar{\theta}_2 = 1$, i.e., two equilibria in the first set disappear. For $\bar{\theta}_2 = \frac{\pi}{2}$, this corresponds to the bifurcation point at $K = 2$. This case is solvable analytically.

#### 4.2.1 Equilibria

Equation (16) at $\bar{\theta}_2 = \frac{\pi}{2}$ becomes

$$K \cos^2 \Psi_2 + \cos \Psi_2 - \frac{K}{2} = 0. \tag{37}$$

We consider first the case that $K \in (0, 2)$. In this case, (37) has two solutions

$$\Psi_2 = \pm \arccos\left(\frac{-1 + \sqrt{1 + 2K^2}}{2K}\right).$$

This and the solutions of (14) give us a total of four equilibria as follows:

1. $\psi_{\text{sync1}} = (\frac{\pi}{2} - \arccos(\frac{-1+\sqrt{1+2K^2}}{2K}), \arccos(\frac{-1+\sqrt{1+2K^2}}{2K}))$.
   By Lemma 3.2, the equilibrium $\psi_{\text{sync1}}$ is a *stable node* for $K \in (0, 2)$.
2. $\psi_{\text{antisync1}} = (\frac{\pi}{2} - \arccos(\frac{-1+\sqrt{1+2K^2}}{2K}), - \arccos(\frac{-1+\sqrt{1+2K^2}}{2K}))$.
   By Lemma 3.3, the equilibrium $\psi_{\text{antisync1}}$ is an *unstable node* for $K \in (0, 2)$.
3. $\psi_{S1} = (\frac{\pi}{2} + \arccos(-\frac{K}{2}), \arccos(-\frac{K}{2}))$.
   By Lemma 3.1, $\psi_{S1}$ is a *saddle point* for all $K \in (0, 2)$.
4. $\psi_{S2} = (\frac{\pi}{2} - \arccos(-\frac{K}{2}), - \arccos(-\frac{K}{2}))$.
   By Lemma 3.1, $\psi_{S2}$ is a *saddle point* for all $K \in (0, 2)$.

We consider next the case that $K > 2$. The equilibria from the first set of solutions are not defined when $K > 2$ and $\bar{\theta}_2 = \frac{\pi}{2}$. Equation (37) in this case has four solutions

$$\Psi_2 = \pm \arccos\left(\frac{-1 \pm \sqrt{1 + 2K^2}}{2K}\right).$$

This gives us a total of four equilibria as follows:

1. $\boldsymbol{\psi}_{\text{sync1}} = (\frac{\pi}{2} - \arccos(\frac{-1+\sqrt{1+2K^2}}{2K}), \arccos(\frac{-1+\sqrt{1+2K^2}}{2K}))$.
   By Lemma 3.2, the equilibrium $\boldsymbol{\psi}_{\text{sync1}}$ is a *stable node* for $K > 2$.

2. $\boldsymbol{\psi}_{\text{antisync1}} = (\frac{\pi}{2} - \arccos(\frac{-1+\sqrt{1+2K^2}}{2K}), -\arccos(\frac{-1+\sqrt{1+2K^2}}{2K}))$.
   By Lemma 3.3, the equilibrium $\boldsymbol{\psi}_{\text{antisync1}}$ is an *unstable node* for $K > 2$.

3. $\boldsymbol{\psi}_{\text{antisync2}} = (\frac{\pi}{2} - \arccos(\frac{-1-\sqrt{1+2K^2}}{2K}), \arccos(\frac{-1-\sqrt{1+2K^2}}{2K}))$.
   By a check of the Jacobian, the equilibrium $\boldsymbol{\psi}_{\text{antisync2}}$ is seen to be a *saddle point* for all $K > 2$.

4. $\boldsymbol{\psi}_{\text{sync2}} = (\frac{\pi}{2} + \arccos(\frac{-1-\sqrt{1+2K^2}}{2K}), -\arccos(\frac{-1-\sqrt{1+2K^2}}{2K}))$.
   By a check of the Jacobian, the equilibrium $\boldsymbol{\psi}_{\text{sync2}}$ is seen to be a *saddle point* for all $K > 2$.

### 4.2.2 Analysis of the bifurcation diagram

The analysis of the previous subsection shows that the bifurcation at $K = 2$ consists in the disappearance of two saddles ($\boldsymbol{\psi}_{S1}$ and $\boldsymbol{\psi}_{S2}$), and the simultaneous appearance of two new saddles ($\boldsymbol{\psi}_{\text{antisync2}}$ and $\boldsymbol{\psi}_{\text{sync2}}$). At the bifurcation, these four equilibria come together at $(\Psi_1, \Psi_2)_{K=2, \bar{\theta}_2 = \frac{\pi}{2}} = (\frac{3\pi}{2}, \pi)$. This equilibrium is highly degenerate; the linearization $J$ is equal to the zero matrix (see Lemma 3.1). This degenerate equilibrium will be encountered again in Sect. 5 when we set $K = 2$ and study bifurcation in the $(\bar{\theta}_2, \Psi_i)$ plane. The $\bar{\theta}_2 = \frac{\pi}{2}$ plane studied here and the $K = 2$ plane studied in Sect. 5 are two orthogonal slices of the full parameter space $(K, \bar{\theta}_2, \Psi_i)$.

### 4.3 Bifurcation in the $(K, \Psi_i)$ Plane for $0 < \bar{\theta}_2 < \frac{\pi}{2}$

The bifurcation diagram in the $(K, \Psi_i)$ plane for $\bar{\theta}_2 = \frac{\pi}{4}$ is plotted in Fig. 4(c). This is representative of the case $0 < \bar{\theta}_2 < \frac{\pi}{2}$. There are two bifurcations: one at $K = K_1$ when two equilibria appear and one at $K = K_0 > K_1$ when two equilibria disappear. For $K_1 < K < K_0$, there are two additional equilibria, but the system still only has one stable equilibrium, unlike the case of $\frac{\pi}{2} < \bar{\theta}_2 < \pi$.

When the two saddles from the first set of solutions disappear, there is no pitchfork, rather the equilibrium from (26), $\boldsymbol{\psi}_{\text{antisync2}}$, switches from being an unstable node to a saddle. To prove this, we consider the linearization of the system near this bifurcation evaluated on the branch of the equilibria corresponding to $\boldsymbol{\psi}_{\text{antisync2}}$. The eigenvalues of the Jacobian are $\lambda_1 = -\cos(\bar{\theta}_2 - \Psi_2)$ and $\lambda_2 = -\cos(\bar{\theta}_2 - \Psi_2) - K\cos(2\Psi_2 - \bar{\theta}_2)$. For $\bar{\theta}_2 < \frac{\pi}{2}$, in some neighborhood of the bifurcation, $\lambda_2 > 0$ since $\lambda_2|_{\boldsymbol{\psi}_0, K_0} = \cot\bar{\theta}_2 > 0$ for $\bar{\theta}_2 < \frac{\pi}{2}$. The eigenvalue $\lambda_1$, as we saw in Sect. 4.1, changes sign through the bifurcation. In order to determine if the change is from positive to negative or negative to positive, we examine how $\Psi_2$ changes as a function of $K$ near the bifurcation. We compute

$$\frac{\partial \Psi_2}{\partial K}\bigg|_{\boldsymbol{\psi}_0, K_0} = -\frac{1}{4}\sin\bar{\theta}_2 \tan\bar{\theta}_2 < 0, \quad \forall\bar{\theta}_2 \in \left(0, \frac{\pi}{2}\right).$$

Hence, $\Psi_2$ is a strictly decreasing function of $K$ around the bifurcation. It is then easy to see that $\lambda_1|_{\psi_{\text{antisync2}}} = -\cos(\bar{\theta}_2 - \Psi_2)|_{\psi_{\text{antisync2}}}$ becomes negative as $K$ crosses the bifurcation value $K_0$. This proves that $\psi_{\text{antisync2}}$ is an unstable node before the bifurcation and a saddle after the bifurcation. Thus, the disappearance of the saddles $\psi_{S1}$ and $\psi_{S2}$ at $K_0$ does not affect the stable equilibria of the system, only the number of unstable equilibria and the type of one unstable equilibrium.

## 5 Bifurcations in the Case $K = 2$

In this section, we set $K = 2$ and study the bifurcations in the $(\bar{\theta}_2, \Psi_i)$ plane. This case is solvable analytically. In model (12), $K = 2$ implies for each subgroup that the strength of the attraction toward the preferred direction is equal to the strength of the attraction to align with the other subgroup. The system (12) dynamics become

$$\dot{\Psi}_1 = -\sin \Psi_1 + \sin(\Psi_2 - \Psi_1),$$
$$\dot{\Psi}_2 = \sin(\bar{\theta}_2 - \Psi_2) - \sin(\Psi_2 - \Psi_1).$$

### 5.1 Equilibria

For $K = 2$, (16) becomes $\sin(\bar{\theta}_2 - \Psi_2) = \sin(2\Psi_2 - \bar{\theta}_2)$. This equation has four solutions,

$$\Psi_2 = \begin{cases} \frac{2}{3}\bar{\theta}_2, \\ \frac{2}{3}\bar{\theta}_2 + \frac{2\pi}{3}, \\ \frac{2}{3}\bar{\theta}_2 + \frac{4\pi}{3}, \\ \pi. \end{cases}$$

The system therefore has a total of six equilibria as follows:

1. $\psi_{\text{sync1}} = (\frac{1}{3}\bar{\theta}_2, \frac{2}{3}\bar{\theta}_2)$.
   By Lemma 3.2, the equilibrium $\psi_{\text{sync1}}$ is a *stable node* for $\bar{\theta}_2 \in [0, \pi]$.
2. $\psi_{\text{sync2}} = (\frac{1}{3}\bar{\theta}_2 - \frac{2\pi}{3}, \frac{2}{3}\bar{\theta}_2 + \frac{2\pi}{3})$.
   By a check of the Jacobian, the equilibrium $\psi_{\text{sync2}}$ is seen to be an *unstable node* for $\bar{\theta}_2 \in [0, \frac{\pi}{2})$ and a *stable node* for $\bar{\theta}_2 \in (\frac{\pi}{2}, \pi]$.
3. $\psi_{\text{antisync1}} = (\frac{1}{3}\bar{\theta}_2 - \frac{4\pi}{3}, \frac{2}{3}\bar{\theta}_2 + \frac{4\pi}{3})$.
   By Lemma 3.3, the equilibrium $\psi_{\text{antisync1}}$ is an *unstable node* for $\bar{\theta}_2 \in [0, \pi]$.
4. $\psi_{\text{antisync2}} = (\bar{\theta}_2 - \pi, \pi)$.
   By a check of the Jacobian, the equilibrium $\psi_{\text{antisync2}}$ is seen to be a *saddle point* for $\bar{\theta}_2 \in [0, \frac{\pi}{2}) \cup (\frac{\pi}{2}, \pi]$.
5. $\psi_{S1} = (\bar{\theta}_2 + \pi, 2\bar{\theta}_2)$.
   By Lemma 3.1, the equilibrium $\psi_{S1}$ is a *saddle point* for all $\bar{\theta}_2 \in [0, \frac{\pi}{2}) \cup (\frac{\pi}{2}, \pi]$.
6. $\psi_{S2} = (-\bar{\theta}_2, \pi)$.
   By Lemma 3.1, the equilibrium $\psi_{S2}$ is a *saddle point* for all $\bar{\theta}_2 \in [0, \frac{\pi}{2}) \cup (\frac{\pi}{2}, \pi]$.
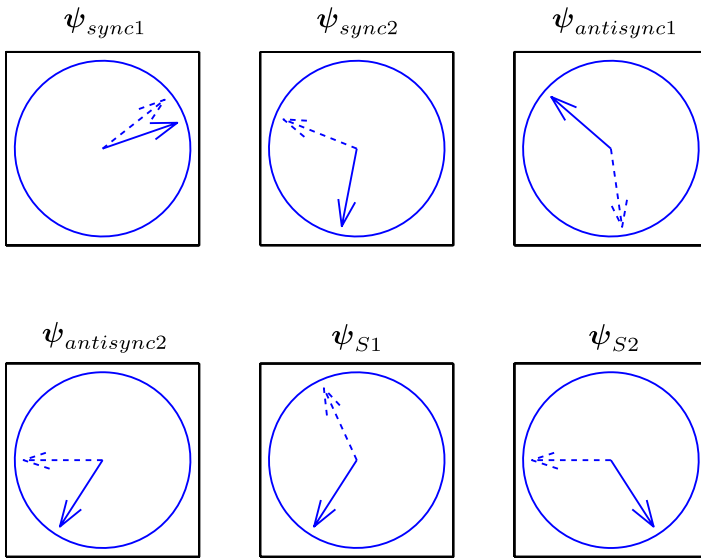
**Fig. 5** Picture of the 6 equilibria for $K = 2$ and $\bar{\theta}_2 = 1$ rad. The *solid arrow* represents $\Psi_1$ on the unit circle, i.e., the average heading of the first informed subgroup, and the *dashed arrow* represents $\Psi_2$, the average heading of the second informed subgroup

Figure 5 shows an example of the six equilibria in the case $K = 2$ and $\bar{\theta}_2 = 1$ rad. The only stable equilibrium is $\psi_{\text{sync1}}$, which for this example corresponds to motion in the $\Psi = 0.5$ rad direction.

## 5.2 Analysis of the Bifurcation Diagram

The analysis of Sect. 5.1 shows that the stability type of one of the equilibria, $\psi_{\text{sync2}}$, changes at $\bar{\theta}_2 = \frac{\pi}{2}$ from an unstable node to a stable node. The equilibrium $\psi_{\text{sync2}}$ for $\bar{\theta}_2 = \frac{\pi}{2}$ is a highly degenerate equilibrium; the Jacobian is equal to the zero matrix. This is the same bifurcation point encountered in Sect. 4.2, but approached from an orthogonal direction in the full parameter space $(K, \bar{\theta}_2, \Psi_i)$. Figure 6 shows the bifurcation diagram in the $(\bar{\theta}_2, \Psi_1)$ plane, i.e., $\Psi_1$ as a function of bifurcation parameter $\bar{\theta}_2$. In the bifurcation diagram (Fig. 6), 4 equilibria come together at the point in phase space $(\Psi_1, \Psi_2) = (\frac{3\pi}{2}, \pi)$ when $\bar{\theta}_2 = \frac{\pi}{2}$. This bifurcation is one of Thom's seven elementary catastrophes; it is called the *elliptic umbilic* (Thom 1972).

Catastrophe theory applies to gradient systems, and the elementary catastrophes are classified by looking at the form of the potential. As discussed in Sect. 2, our system obeys gradient dynamics and the associated potential for $K = 2$ is

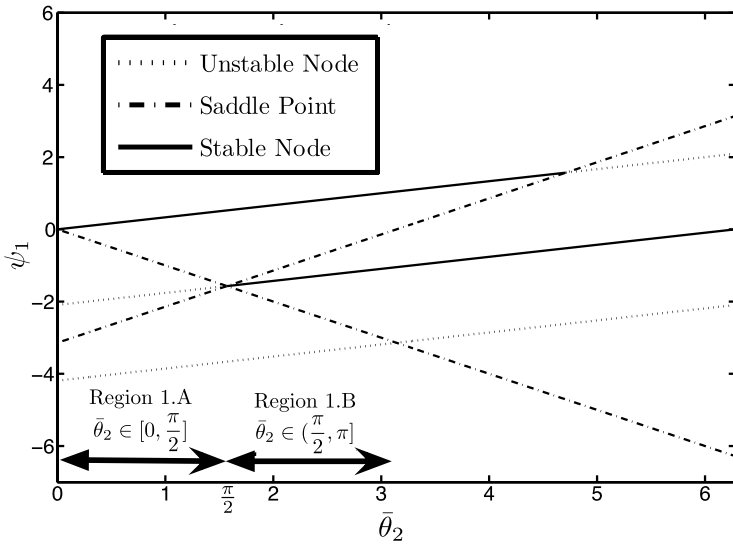$$V = \cos\Psi_1 + \cos(\bar{\theta}_2 - \Psi_2) + \cos(\Psi_1 - \Psi_2). \tag{38}$$

**Fig. 6** Bifurcation diagram in the $(\bar{\theta}_2, \Psi_1)$ plane, i.e., $\Psi_1$ as a function of bifurcation parameter $\bar{\theta}_2$ fixing $K = 2$. Since the equilibria $\psi_{\text{antisync2}}$ and $\psi_{S1}$ have the same value for $\Psi_1$ (but a different value for $\Psi_2$), we see on this diagram only 5 equilibria even though there are six. At $\bar{\theta}_2 = \frac{\pi}{2}$, there are only three distinct equilibria; this is the degenerate point of the system. The multiplicity of the equilibrium $(\frac{3\pi}{2}, \pi)$ is four

To identify the bifurcation as an elliptic umbilic, we examine the unfolding of this potential near the catastrophe $(\Psi_1, \Psi_2, \bar{\theta}_2) = (\frac{3\pi}{2}, \pi, \frac{\pi}{2})$. We write (38) as

$$V = \cos\left(u + \frac{3\pi}{2}\right) + \cos\left(\frac{\pi}{2} + a - (\pi + v)\right) + \cos\left(u + \frac{3\pi}{2} - (\pi + v)\right), \quad (39)$$

where $u$, $v$, and $a$ are respectively the deviation of $\Psi_1$ from $\frac{3\pi}{2}$, $\Psi_2$ from $\pi$, and $\bar{\theta}_2$ from $\frac{\pi}{2}$. A Taylor expansion of (39), keeping terms up to third order in $u$ and $v$ gives

$$V = \frac{(\cos a - 1)}{3!}v^3 + \frac{uv^2}{2} - \frac{vu^2}{2} - \frac{\sin a}{2}v^2 + (1 - \cos a)v + \sin a.$$

After the following change of variables:

$$x = \frac{1}{2}\sqrt[3]{\frac{(4\cos a - 1)}{3}}v,$$

$$y = \sqrt[3]{\frac{2\sqrt{6}}{\sqrt{4\cos a - 1}}}\left(\frac{1}{\sqrt{6}}u - \frac{1}{2\sqrt{6}}v\right),$$

the potential becomes

$$V = x^3 - 3xy^2 - \frac{2 \times 3^{\frac{2}{3}}\sin a}{(4\cos a - 1)^{\frac{2}{3}}}x^2 - \frac{2 \times 3^{\frac{1}{3}}(\cos a - 1)}{(4\cos a - 1)^{\frac{1}{3}}}x + \sin a. \quad (40)$$

$\boldsymbol{\psi}_{sync1}$ $\qquad$ $\boldsymbol{\psi}_{sync2}$ $\qquad$ $\boldsymbol{\psi}_{antisync1}$

$\boldsymbol{\psi}_{antisync2}$ $\qquad$ $\boldsymbol{\psi}_{S1}$ $\qquad$ $\boldsymbol{\psi}_{S2}$
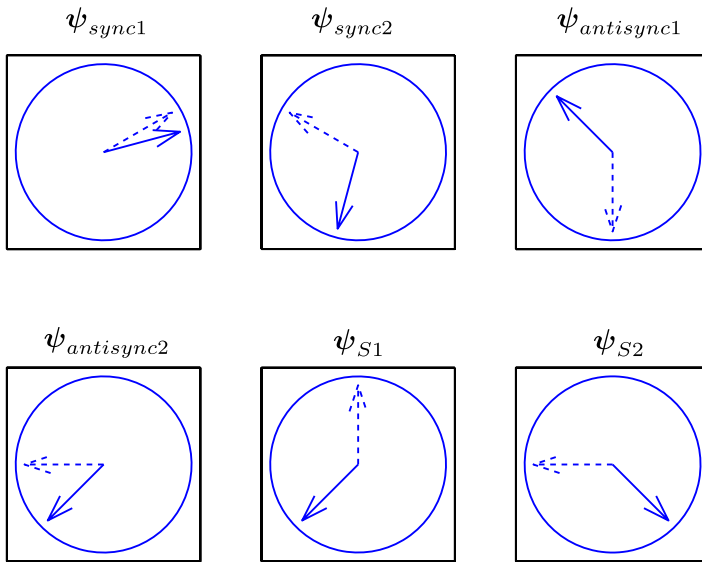


**Fig. 7** These diagrams show pictures of all the equilibria for $\bar{\theta}_2 = \frac{\pi}{4}$. This is representative of the possible equilibria for the system in Region 1A without its boundary, i.e., for $\bar{\theta}_2 \in [0, \frac{\pi}{2})$. The only stable equilibrium is $\boldsymbol{\psi}_{\text{sync1}}$, which for this example corresponds to motion in the $\Psi = \frac{\pi}{8}$ direction

In (40), we recognize the standard unfolding of the potential of an elliptic umbilic (Poston and Stewart 1978).

In the following, we examine the different equilibria in each of the various regions of the bifurcation diagram shown in Fig. 6. Region 1.A is defined by $\bar{\theta}_2 \in [0, \frac{\pi}{2}]$ and Region 1.B by $\bar{\theta}_2 \in [\frac{\pi}{2}, \pi]$. For each case studied, we draw the pictures of each possible equilibrium (stable and unstable) on the unit circle, a solid arrow corresponding to $\Psi_1$ and a dashed arrow corresponding to $\Psi_2$. Because $K = 2$ implies equal attraction to the preferred direction as to the other subgroup, equilibria are usually not fully synchronized nor antisynchronized. Instead, the equilibria $\boldsymbol{\psi}_{\text{sync1}}$ and $\boldsymbol{\psi}_{\text{sync2}}$ are *K-almost synchronized* and $\boldsymbol{\psi}_{\text{antisync1}}$ and $\boldsymbol{\psi}_{\text{antisync2}}$ are *K-almost antisynchronized*. Since $\boldsymbol{\psi}_{S1}$ and $\boldsymbol{\psi}_{S2}$ from (14) are not defined for $K \gg 1$, we cannot use this terminology. However, we note that the relative heading of $\Psi_1$ with respect to $\Psi_2$ is equal to $\pi - \bar{\theta}_2$ for $\boldsymbol{\psi}_{S1}$ and $\pi + \bar{\theta}_2$ for $\boldsymbol{\psi}_{S2}$ independent of $K$. As $\bar{\theta}_2$ increases to $\pi$, the two saddles become synchronized. We call an equilibrium $\bar{\theta}_2$-*almost synchronized* if the corresponding equilibrium is synchronized in the case $\bar{\theta}_2 \to \pi$.

*Region 1.A* $\bar{\theta}_2 \in [0, \frac{\pi}{2}]$. The equilibria in the case $\bar{\theta}_2 \in [0, \frac{\pi}{2})$ are shown in Fig. 7. Figure 8 shows the equilibria at the bifurcation point $\bar{\theta}_2 = \frac{\pi}{2}$. In Fig. 7, there are three types of equilibria: the $K$-almost synchronized $\boldsymbol{\psi}_{\text{sync1}}$ and $\boldsymbol{\psi}_{\text{sync2}}$, the $K$-almost antisynchronized $\boldsymbol{\psi}_{\text{antisync1}}$ and $\boldsymbol{\psi}_{\text{antisync2}}$ and the $\bar{\theta}_2$-almost synchronized $\boldsymbol{\psi}_{S1}$ and $\boldsymbol{\psi}_{S2}$. The only stable equilibrium, $\boldsymbol{\psi}_{\text{sync1}}$, is the $K$-almost synchronized motion of $\Psi_1$ and $\Psi_2$ in the direction $\Psi = \frac{\bar{\theta}_2}{2}$ with each heading remaining on its side (nearest its preferred direction) of $\Psi = \frac{\bar{\theta}_2}{2}$. The unstable equilibria are the two $K$-almost antisynchronized $\boldsymbol{\psi}_{\text{antisync1}}$ and $\boldsymbol{\psi}_{\text{antisync2}}$, the remaining $K$-almost synchronized $\boldsymbol{\psi}_{\text{sync2}}$

$$\psi_{sync1} \qquad \psi_{sync2}, \psi_{antisync2}, \psi_{S1}, \psi_{S2} \qquad \psi_{antisync1}$$
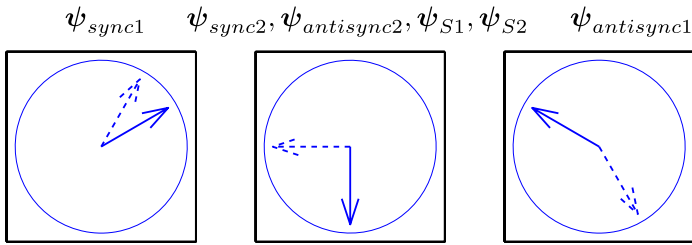


**Fig. 8** These diagrams show the equilibria of the system at the critical point, i.e., when both $K = 2$ and $\bar{\theta}_2 = \frac{\pi}{2}$. We only have 3 equilibria. The second equilibrium drawn is the superposition of 4 equilibria $\psi_{sync2}, \psi_{antisync2}, \psi_{S1}$ and $\psi_{S2}$; it has multiplicity four. It is called a monkey-saddle in the catastrophe theory literature

which flanks $\Psi = \frac{\bar{\theta}_2}{2} + \pi$ and the two $\bar{\theta}_2$-almost synchronized saddles. As $\bar{\theta}_2 \to \pi$, the first saddle $\psi_{S1}$ will tend to go closer to the preferred direction $\bar{\theta}_1 = 0$, and the second saddle $\psi_{S2}$ will go closer to $\bar{\theta}_2$.

As mentioned previously, the case at the boundary $\bar{\theta}_2 = \frac{\pi}{2}$ is highly degenerate. There are only three distinct equilibria. There is still only one stable equilibrium which is $K$-almost synchronized at $\Psi = \frac{\bar{\theta}_2}{2} = \frac{\pi}{4}$. There is also an unstable $K$-almost antisynchronized equilibrium $\psi_{antisync1}$ at $\Psi = \frac{\bar{\theta}_2}{2} + \pi = \frac{5\pi}{4}$. The other equilibrium corresponds to $\Psi = \frac{\bar{\theta}_2}{2} + \pi = \frac{5\pi}{4}$. As can be seen in the bifurcation diagram of Fig. 6, there is the superposition of four equilibria $\psi_{sync2}$, $\psi_{S1}$, $\psi_{S2}$, and $\psi_{antisync2}$. This equilibrium is called a *monkey-saddle* in the catastrophe theory literature (Poston and Stewart 1978).

*Region 1.B* $\bar{\theta}_2 \in (\frac{\pi}{2}, \pi]$. The equilibria in the case $\bar{\theta}_2 \in (\frac{\pi}{2}, \pi)$ are shown in Fig. 9. Figure 10 shows the equilibria at the boundary $\bar{\theta}_2 = \pi$. In Fig. 9, the equilibria are similar to those from the case where $\bar{\theta}_2 \in [0, \frac{\pi}{2})$ in Fig. 7 except that now the $K$-almost synchronized equilibrium $\psi_{sync2}$ at $\frac{\bar{\theta}_2}{2} + \pi$ is stable. Two of the unstable equilibria ($\psi_{antisync1}, \psi_{antisync2}$) are $K$-almost anti-synchronized. As mentioned above, for $\psi_{S1}$ and $\psi_{S2}$, the particles synchronize as $\bar{\theta}_2$ increases; the saddle $\psi_{S1}$ is closer to the preferred direction of the first particle and the saddle $\psi_{S2}$ is closer to the preferred direction of the second particle.

In the case $\bar{\theta}_2 = \pi$ (Fig. 10), there are still two stable equilibria ($\psi_{sync1}, \psi_{sync2}$) which are $K$-almost synchronized at $\Psi = \frac{\bar{\theta}_2}{2} = \frac{\pi}{2}$ and $\Psi = \frac{\bar{\theta}_2}{2} + \pi = \frac{3\pi}{2}$, respectively. The unstable equilibria $\psi_{antisync1}$ and $\psi_{antisync2}$ are antisynchronized. The two saddles are synchronized: $\psi_{S1}$ is synchronized at the preferred direction of the first particle ($\bar{\theta}_1 = 0$) and $\psi_{S2}$ is synchronized at the preferred direction of the second particle ($\bar{\theta}_2 = \pi$).

## 6 Bifurcation in the $(K, \Psi_i)$ Plane for $\bar{\theta}_2 = \pi$

In this section, we set $\bar{\theta}_2 = \pi$, and study the bifurcation in the $(K, \Psi_i)$ plane. This case is solvable analytically. For this case, the two preferred headings differ by 180

$\psi_{sync1}$        $\psi_{sync2}$        $\psi_{antisync1}$

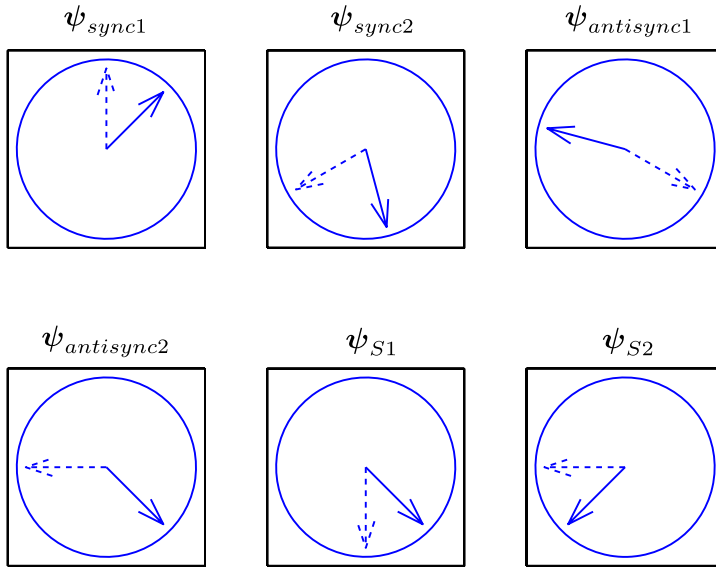$\psi_{antisync2}$        $\psi_{S1}$        $\psi_{S2}$

**Fig. 9** These diagrams show the pictures of all the equilibria for $\bar{\theta}_2 = \frac{3\pi}{4}$. This is representative of the possible equilibria for the system in Region 1B without its boundary, i.e., for $\bar{\theta}_2 \in (\frac{\pi}{2}, \pi)$. The two saddles, $\psi_{S1}$ and $\psi_{S2}$, tend to be more synchronized (than in Fig. 7) since $\bar{\theta}_2$ is closer to $\pi$. $\psi_{S1}$ is closer to the preferred direction of the first subgroup and $\psi_{S2}$ is closer to the preferred direction of the second subgroup. There are two stable equilibria, $\psi_{sync1}$ and $\psi_{sync2}$

degrees. Since the disagreement is so large, for some range of small values of $K$ the group will split without making any compromise. This kind of splitting is sometimes observed in swarm-bees (Lindauer 1957). The system (12) becomes

$$
\begin{aligned}
\dot{\Psi}_1 &= -\sin\Psi_1 + \frac{K}{2}\sin(\Psi_2 - \Psi_1), \\
\dot{\Psi}_2 &= \sin\Psi_2 + \frac{K}{2}\sin(\Psi_1 - \Psi_2).
\end{aligned}
\tag{41}
$$

We note that this system appears in Chap. 8 of (Strogatz 1994).

### 6.1 Equilibria

For $\bar{\theta}_2 = \pi$, (16) becomes

$$
\sin\Psi_2(1 + K\cos\Psi_2) = 0.
\tag{42}
$$

We consider first the case that $K \in [0, 1)$. In this case, (42) has two solutions

$$
\Psi_2 = \begin{cases} 0, \\ \pi. \end{cases}
$$

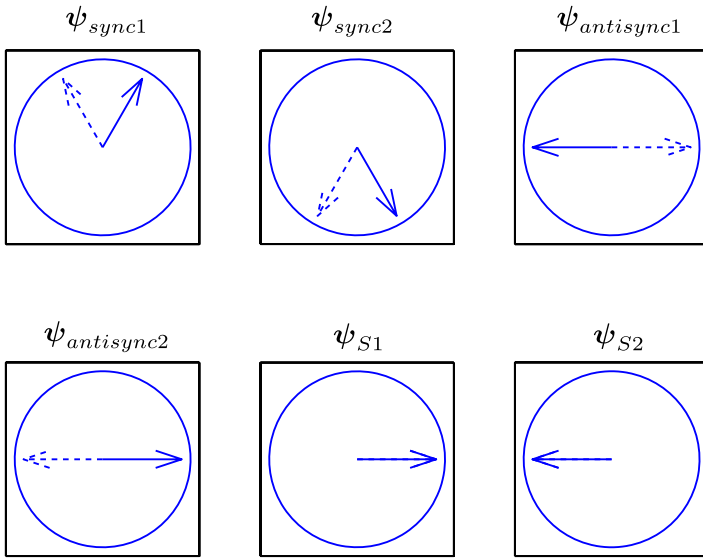This give us a total of 4 equilibria as follows.

**Fig. 10** These diagrams show the equilibria of the system at the right boundary of Region 1.B, i.e., for $\bar{\theta}_2 = \pi$. Only equilibrium $\psi_{\text{sync1}}$ and $\psi_{\text{sync2}}$ (the $K$-almost synchronized equilibria) depend on $K$. The other equilibria are antisynchronized ($\psi_{\text{antisync1}}$ and $\psi_{\text{antisync2}}$) or synchronized ($\psi_{S1}$ and $\psi_{S2}$) for all $K$

1. $\psi_{\text{antisync1}} = (\pi, 0)$.
   By Lemma 3.3, the equilibrium $\psi_{\text{antisync1}}$ is an *unstable node* for $K \in [0, 1]$.
2. $\psi_{\text{antisync2}} = (0, \pi)$.
   By a check of the Jacobian, the equilibrium $\psi_{\text{antisync2}}$ is seen to be a *stable node* $\forall K \in [0, 1)$.
3. $\psi_{S1} = (0, 0)$.
   By Lemma 3.1, the equilibrium $\psi_{S1}$ is a *saddle point* for all $K \in [0, 1]$.
4. $\psi_{S2} = (\pi, \pi)$.
   By Lemma 3.1, the equilibrium $\psi_{S2}$ is a *saddle point* for all $K \in [0, 1]$.

We consider next the case that $K > 1$. Equation (42) in this case has four solutions

$$
\Psi_2 = \begin{cases}
\arccos(-\frac{1}{K}), \\
-\arccos(-\frac{1}{K}), \\
0, \\
\pi.
\end{cases}
$$

This gives a total of six equilibria as follows:

1. $\psi_{\text{sync1}} = (\pi - \arccos(-\frac{1}{K}), \arccos(-\frac{1}{K}))$.
   By Lemma 3.2, the equilibrium $\psi_{\text{sync1}}$ is a *stable node* for $K > 1$.
2. $\psi_{\text{sync2}} = (\pi + \arccos(-\frac{1}{K}), -\arccos(-\frac{1}{K}))$.
   By a check of the Jacobian, the equilibrium $\psi_{\text{sync2}}$ is seen to be a *stable node* $\forall K > 1$.

**Fig. 11** Bifurcation diagram in the $(K, \Psi_1)$ plane, i.e., $\Psi_1$ as a function of bifurcation parameter $K$ fixing $\bar{\theta}_2 = \pi$. At $K = 1$, we have a supercritical pitchfork bifurcation. We have one stable equilibrium for $K < 1$ and two stable equilibria for $K > 1$
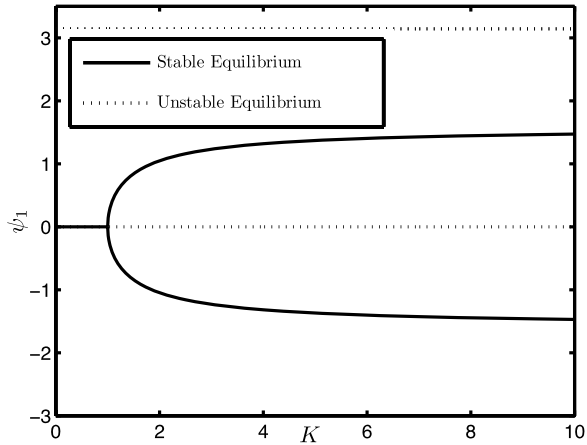


3. $\boldsymbol{\psi}_{\text{antisync1}} = (\pi, 0)$.
   By Lemma 3.3, the equilibrium $\boldsymbol{\psi}_{\text{antisync1}}$ is an *unstable node* for $K \geq 1$.
4. $\boldsymbol{\psi}_{\text{antisync2}} = (0, \pi)$.
   By a check of the Jacobian, the equilibrium $\boldsymbol{\psi}_{\text{antisync2}}$ is seen to be a *saddle point* $\forall K > 1$.
5. $\boldsymbol{\psi}_{S1} = (0, 0)$.
   By Lemma 3.1, the equilibrium $\boldsymbol{\psi}_{S1}$ is a *saddle point* for all $K \geq 1$.
6. $\boldsymbol{\psi}_{S2} = (\pi, \pi)$.
   By Lemma 3.1, the equilibrium $\boldsymbol{\psi}_{S2}$ is a *saddle point* for all $K \geq 1$.

### 6.2 Analysis of the bifurcation diagram

The analysis of the previous subsection shows that a bifurcation occurs at $K = 1$. The bifurcation diagram (Fig. 11) suggests that there is a *supercritical pitchfork bifurcation*. To prove this, we use the extension for pitchforks of the general theorem for saddle node bifurcations in (Guckenheimer and Holmes 1983). There are three conditions to check in the theorem. We define $\boldsymbol{\psi}_0 = (\Psi_1, \Psi_2)_0 = (0, \pi)$, $K_0 = 1$.

1. *Nondegeneracy of the linearization.*
   The linearization of (41) at $\boldsymbol{\psi} = \boldsymbol{\psi}_0$ and $K = K_0$ is

$$J_0 = \left.\frac{\partial \mathbf{f}}{\partial \boldsymbol{\psi}}\right|_{\boldsymbol{\psi}_0, K_0} = \begin{pmatrix} -\frac{1}{2} & -\frac{1}{2} \\ -\frac{1}{2} & -\frac{1}{2} \end{pmatrix},$$

   where $\mathbf{f}$ is the vector field given by (41) with corresponding state vector $\boldsymbol{\psi} = (\Psi_1, \Psi_2)$. This linearization is nondegenerate since it has a simple zero eigenvalue. We set $v = \begin{pmatrix} 1 \\ -1 \end{pmatrix}$ and $w = (1 \ -1)$ to be respectively the right and left eigenvectors for the zero eigenvalue.

2. *Transversality condition to control nondegeneracy with respect to the parameter.*
   We compute

$$\frac{\partial^2 \mathbf{f}}{\partial \boldsymbol{\psi} \partial K}\bigg|_{\boldsymbol{\psi}_0, K_0} = \frac{1}{2} \begin{pmatrix} 1 & -1 \\ -1 & 1 \end{pmatrix},$$

   which implies that $w.\frac{\partial^2 \mathbf{f}}{\partial \boldsymbol{\psi} \partial K}|_{\boldsymbol{\psi}_0, K_0}.v = 2 \neq 0$. Hence, the eigenvalues cross the imaginary axis with nonzero speed which proves the condition.

3. *Transversality condition to control nondegeneracy with respect to the dominant effect of the cubic nonlinear term.*
   For this condition, we compute

$$w_i v_j v_k v_l \frac{\partial^3 f_i}{\partial \Psi_j \partial \Psi_k \partial \Psi_l}\bigg|_{\boldsymbol{\psi}_0, K_0} = -6 < 0,$$

   for all $i, j, k, l \in \{1, 2\}$ and $f_i$ is the $i$th component of $\mathbf{f}$. Since we get a strictly negative number, the pitchfork is supercritical.

This last condition completes the proof of the existence of a codimension-one supercritical pitchfork bifurcation at $\boldsymbol{\psi} = (0, \pi)$, $K = 1$.

Before the bifurcation ($K < 1$), the only stable equilibrium is $\boldsymbol{\psi}_{\text{antisync2}} = (0, \pi)$. This corresponds to the case where each informed subgroup follows its own preferred direction; there is no compromise between the individuals and the group splits. When $K < 1$, the strength of the coupling force compared to the preferred direction is too weak to influence the stable steady state of the system. The motion of the group is the same as if there were no coupling between the two informed subgroups. For $K > 1$, there are two stable equilibria, $\boldsymbol{\psi}_{\text{sync1}}$ and $\boldsymbol{\psi}_{\text{sync2}}$. These correspond, respectively, to the motion in the directions $\Psi = \frac{\bar{\theta}_2}{2} = \frac{\pi}{2}$ and $\Psi = \frac{\bar{\theta}_2}{2} + \pi = \frac{3\pi}{2}$. As we increase the bifurcation parameter $K$, the two directions $\Psi_1$ and $\Psi_2$ become synchronized. $\bar{\theta}_2 = \pi$ is the only case where we have two stable equilibria for large value of $K$.

## 7 Interpretation and Extensions of Results

We have modeled and studied equilibria, stability, and bifurcations for a group of $N = N_1 + N_2 + N_3$ coupled individuals moving in the plane where there are $N_1$ informed individuals with a preferred direction $\bar{\theta}_1 = 0$, $N_2 = N_1$ informed individuals with a second preferred direction $\bar{\theta}_2$ and $N_3 = 0$ uninformed individuals. We showed that the system has either one or two stable equilibria. The $K$-almost synchronized motion ($\boldsymbol{\psi}_{\text{sync1}}$) of the two subgroups in the direction $\Psi = \frac{\bar{\theta}_2}{2}$ is always stable. This corresponds to the whole group moving together (when $K$ is large) in the average of the two preferred directions. This is consistent with the results in the paper (Couzin et al. 2005) for the case that $\bar{\theta}_2$ is below a threshold, i.e., the disagreement in preferred directions between the two informed subgroups is not too large. This threshold, which depends on system parameters, can be fairly substantial; in the first case, illustrated in Fig. 3 of (Couzin et al. 2005), the threshold is somewhat larger than $2\pi/3$ degrees.
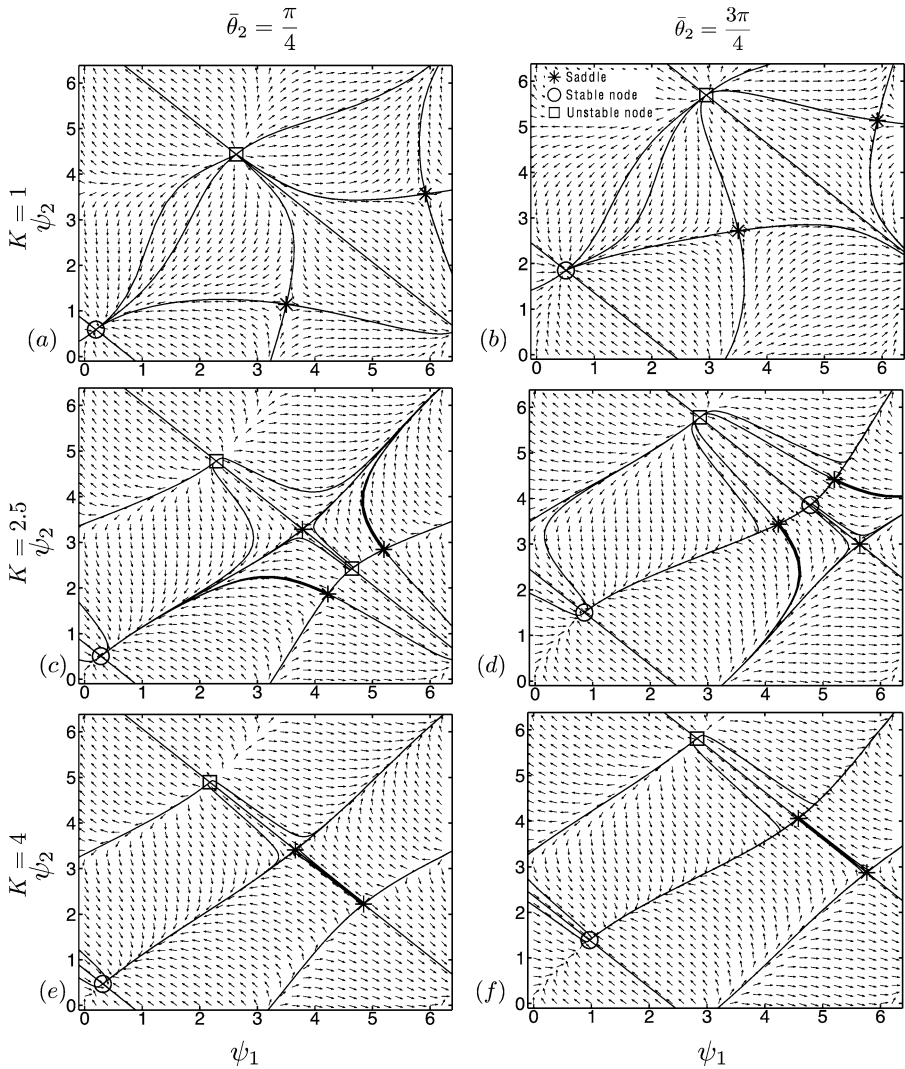
**Fig. 12** Phase portrait for heading directions $\Psi_1$ and $\Psi_2$ at three different values of $K$ and two different values of $\bar{\theta}_2$

For $K \in (K_1, K_0)$ and $\bar{\theta}_2 \in [\frac{\pi}{2}, \pi)$, the $K$-almost synchronized motion ($\boldsymbol{\psi}_{\text{sync2}}$) of the two subgroups in the direction $\Psi = \frac{\bar{\theta}_2}{2} + \pi$ is also stable. This corresponds to the whole group moving together (when $K$ is large) in the opposite of the average of the two preferred directions. The region of attraction for this equilibrium may be relatively small and this can explain why this stable solution was not discovered in the simulation study of (Couzin et al. 2005); see, for example, the middle, right plot in Fig. 12 and the bell-shaped region of attraction around the stable node located near the point $(4.8, 3.8)$. We showed that this stable node appears at a hypercritical pitchfork bifurcation at $\boldsymbol{\psi}_0 = (\frac{3\pi}{2}, \bar{\theta}_2 + \frac{\pi}{2})$, $K = 2/\sin \bar{\theta}_2$ when $\bar{\theta}_2 \in [\frac{\pi}{2}, \pi)$. We also

showed that this stable node disappears at the highly degenerate bifurcation point $\boldsymbol{\psi}_0 = (\frac{3\pi}{2}, \pi)$, $K = 2$ and $\bar{\theta}_2 = \frac{\pi}{2}$, where the linearization is equal to the zero matrix. This bifurcation was investigated in the $(\bar{\theta}_2, \Psi_i)$ plane and was shown to be an elliptic umbilic catastrophe.

Figure 12 shows the phase portrait for the subgroup heading directions $\Psi_1$ and $\Psi_2$ for two values of $\bar{\theta}_2$ and three values of $K$. The vertical (and likewise horizontal) edges are identified since the phase space is the torus. Some of the stable and unstable manifolds are plotted as solid lines and the vector field is plotted as arrows so that the flow can be readily observed. For example, as described above, in the right, middle plot, these manifolds illustrate the region of attraction for the second stable equilibrium $\boldsymbol{\psi}_{\mathrm{sync2}}$. The middle plots together show before (left) and after (right) the elliptic umbilic catastrophe. The three panels in the left column, corresponding to $\bar{\theta}_2 = \pi/4$, show equilibria that can also be observed in the bifurcation plot of Fig. 4(c) at $K = 1$ for the top plot, $K = 2.5$ for the middle plot, and $K = 4$ for the bottom plot. For example, the single stable equilibrium can be observed to be near the point $\Psi_1 = \Psi_2 = \pi/8$, i.e., the $K$-almost synchronized equilibrium $\boldsymbol{\psi}_{\mathrm{sync1}}$ at $\bar{\theta}_2/2 = \pi/8$. Likewise, the three panels in the right column, corresponding to $\bar{\theta}_2 = 3\pi/4$, show equilibria that can also be observed in the bifurcation plot of Fig. 4(a) at $K = 1$ for the top plot, $K = 2.5$ for the middle plot, and $K = 4$ for the bottom plot.

We illustrate in Fig. 13 the dynamics near one of the instabilities with a simulation in the case $N_1 = N_2 = 5$. Snapshots of the positions and heading directions of all 10 individuals are shown at three different times in the three left column plots. The corresponding heading directions of all 10 individuals are plotted on the unit circle together with the preferred heading directions in the right column plots. The initial condition, shown in Figs. 13(a) and (b) is close to the saddle point $\boldsymbol{\psi}_{\mathrm{sync2}}$ shown in the bottom right plot of Fig. 12, i.e., the individuals are heading in the opposite direction of the compromise of the preferred directions. First, as expected (but not shown in Fig. 13), the individuals with the same preferred direction synchronize. Then more slowly, the two lumped subgroups both move away from the unstable solution (in the counter-clockwise direction around the unit circle). Figures 13(c) and (d) show that they are close together as they move and practically all synchronized as they pass through the preferred direction of subgroup 1. Figures 13(e) and (f) show the convergence to the stable solution $\boldsymbol{\psi}_{\mathrm{sync1}}$.

In (Couzin et al. 2005) for $\bar{\theta}_2$ greater than a threshold (e.g., a threshold of $2\pi/3$ in the example cited above), the group was observed to move together in one or the other of the two preferred directions. Our model does not reproduce this result although there are similarities in our model in the case in which $\bar{\theta}_2 = \pi$, i.e., when the two preferred directions are exactly opposite. In this case, there is a supercritical pitchfork at $\boldsymbol{\psi}_0 = (0, \pi)$, $K = 1$. Here, for $K < 1$, each informed subgroup moves stably in its own preferred direction, while for $K > 1$, the two subgroups move together (when $K$ is large) in the average of the preferred directions (i.e., $\pi/2$).

In the case $N_1 \neq N_2$, the persistent stable equilibrium does not correspond to $\Psi = \frac{\bar{\theta}_2}{2}$, but rather to a weighted average of 0 and $\bar{\theta}_2$. For example, if $N_1 > N_2$, the stable solution $\Psi$ corresponds to a direction closer to 0 than to $\bar{\theta}_2$. For $N_2$ fixed, the stable equilibrium value of $\Psi$ asymptotically approaches 0 for increasing $N_1$ as shown in
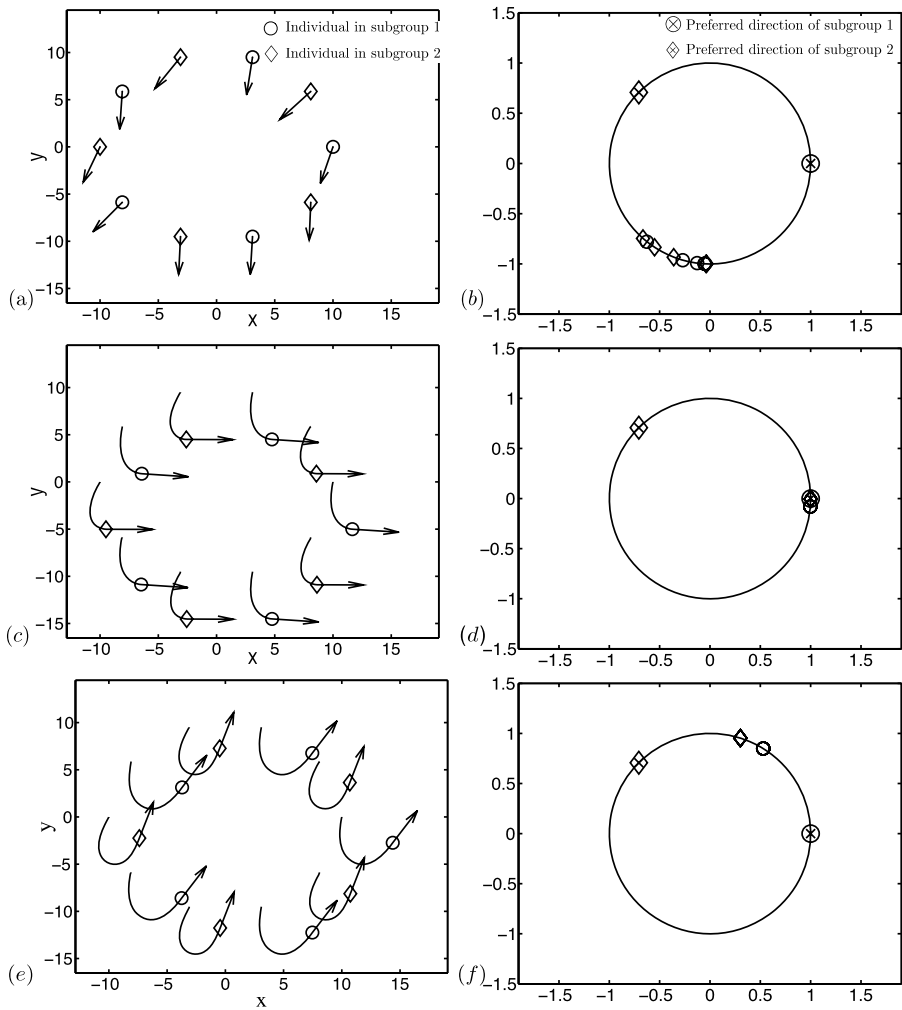
**Fig. 13** Simulation for two informed subgroups each with a population of five individuals ($N_1 = N_2 = 5$). The *plots in the left column* show snapshots in the physical plane of the individual positions $r_j$, $j = 1, \ldots, 10$ (circles for individuals in subgroup 1 and diamonds for individuals in subgroup 2) and individual headings $\theta_j$, $j = 1, \ldots, 10$ (arrows). The *plots in the right column* show the individual headings plotted on the unit circle together with the two preferred directions. The headings of the individuals are initially near the (unstable) equilibrium $\psi_{\text{sync2}}$ with $K = 70$, $\bar{\theta}_2 = \frac{3\pi}{4}$. (**a**) and (**b**) correspond to initial time $t = 0$. (**c**) and (**d**) correspond to time $t = 11.73$. (**e**) and (**f**) correspond to time $t = 19.16$

Fig. 14. Likewise for $N_1$ fixed, the stable equilibrium value of $\Psi$ asymptotically approaches $\bar{\theta}_2$ for increasing $N_2$.

## 8 Conclusion

We have presented and studied a continuous-time model of a mobile, multi-agent system in which individuals in the group balance an interest in moving in the same

**Fig. 14** (**a**) The equilibrium values of $\Psi_1$ and $\Psi_2$ corresponding to the stable motion $\boldsymbol{\psi}_{\text{sync1}}$ as a function of subgroup population size $N_1$ for fixed subgroup population size $N_2 = 5$. As $N_1$ increases the stable equilibrium values of both $\Psi_1$ and $\Psi_2$ approach 0, the preferred direction $\bar{\theta}_1$ of the subgroup with dominating population size $N_1$. (**b**) The stable equilibrium $\boldsymbol{\psi}_{\text{sync1}}$ for the two extreme values of $N_1$. The motion of the group is closer to $\bar{\theta}_2 = 2$ rad when $1 = N_1 < N_2 = 5$. The motion of the group is closer to $\bar{\theta}_1 = 0$ rad when $50 = N_1 > N_2 = 5$



(a)



(b)
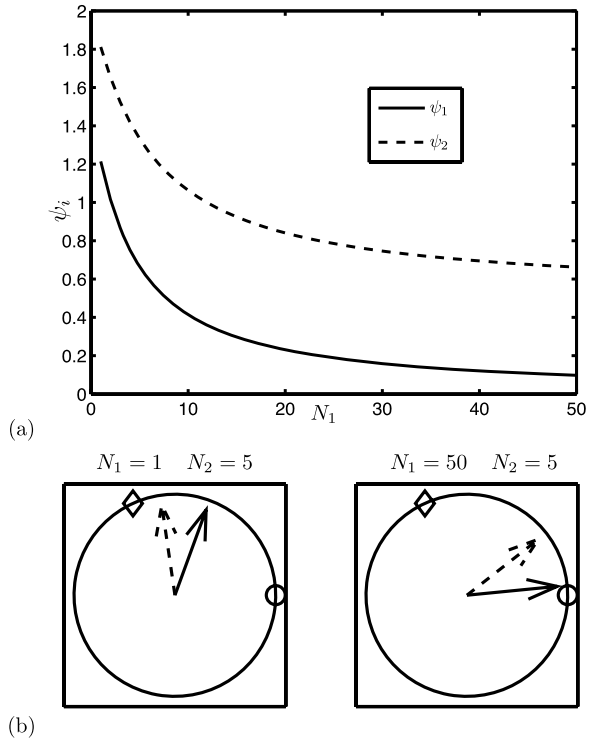
direction as others with an interest in moving in a preferred direction. The model provides a mathematical framework to explore mechanisms at the level of the individual that are critical to the macroscopic behavior observed in the study of collective animal decision making and leadership in (Couzin et al. 2005).

Our model assumes some homogeneity in the group; however, in (Moon et al. 2007), extensions of this homogeneous model are investigated by introducing heterogeneity. Heterogeneity is considered both in the context of informed and uninformed individuals. With either type of heterogeneity, both the time-scale separation and the lumped behavior remain unchanged. Indeed some of the very same bifurcations proven in the present paper are recovered numerically in (Moon et al. 2007) suggesting a measure of robustness to the results here.

The continuous-time model in this paper presents several simplifications as compared to the discrete-time model in (Couzin et al. 2005). First, we constrain our study to the phase dynamics of the individuals rather than the full spatial dynamics. Also, we assume that the individuals can be influenced by all other individuals (not just ones nearby). Finally, we perform the bifurcation analysis of the system in the absence of uninformed individuals and without a forgetting factor feedback term used in (Couzin et al. 2005). Our continuous-time model, like the discrete-time model in (Couzin et al. 2005), shows that consensus is possible within a group of individuals with conflicting information and without signaling or identification of informed individuals. However, unlike the discrete-time model with uninformed individuals, the continuous-time model restricted to informed individuals only (i.e., $N_3 = 0$) and

without the forgetting factor does not exhibit full synchronization of the group unless the coupling gain $K$ is very large (equivalent to the weight $\omega$ of the preferred direction in (Couzin et al. 2005) being very small). This means that for relatively small weight on the coupling in the model (1) with $N_3 = 0$, the individuals in the population do not fully aggregate and the group splits. Also it never happens, in the case of equal populations for the two informed subgroups ($N_1 = N_2$) that the group selects to move as a whole in one of the preferred directions.

On the other hand, if we introduce a forgetting factor feedback in the form of a dynamic gain on the relative strength of the attraction to the preferred direction, analogous to the feedback on the weight $\omega$ in (Couzin et al. 2005), which reinforces (diminishes) the gain if individuals find themselves moving in (away from) their preferred direction, then simulation results resemble more closely those in (Couzin et al. 2005). That is, there is consensus without a large $K$ and the group can choose one or the other of the preferred directions.

The results of (Couzin et al. 2005) show that the forgetting factor should not be necessary for the fundamental behavior. This suggests a possibly interesting role for the naive individuals and limited communication, which we are investigating both in simulation and with extensions to the model. For example, we might expect that as a function of initial conditions, the uninformed individuals could be "won over" by one of the two informed subgroups. Then in effect, the "winning" informed subgroup will appear in the model to have its membership greatly increased. In this case, just like the case $N_1 > N_2$ discussed above, the group will move in a weighted average direction that is close to the preferred direction as long as the number of uninformed individuals is large as compared to uninformed individuals in the "losing" subgroup. The dependency on the angle between the two preferred directions revealed in the discrete-time model might also be reasonably recovered with the inclusion of uninformed individuals. For small differences in preferred direction, it might be that the uninformed individuals are not won over by either informed subgroup and instead contribute to consensus at the average, whereas at large differences between preferred directions, the discussion above might apply so that the group effectively picks one of the preferred directions.

As the continuous-time model grows to better resemble the behavior of the natural system, the value of the modeling and analysis will increase. Prediction of stability and bifurcation of solutions, analogous to those in the present paper, have the potential to provide new insights by going beyond regions of phase space explored with discrete simulation. In this paper, we have laid mathematical foundations and developed insights that contribute to the general interest in isolating a biologically plausible mechanism for the collective decision-making behavior as observed in (Couzin et al. 2005) when there is conflicting information among agents.

## Appendix A:  Proof of Well-Defined Change of Variables

In this appendix, we show that the change of variables $\boldsymbol{\theta} \mapsto (\boldsymbol{\alpha}^1, \Psi_1, \boldsymbol{\alpha}^2, \Psi_2, \boldsymbol{\alpha}^3, \Psi_3)$ from Sect. 2.2 is well defined near the manifold $\mathcal{M}$, where $\mathcal{M}$ is the invariant man-

ifold of (1) defined by $\theta_j = \Psi_k$, $j \in \mathcal{N}_k$, $k = 1, 2, 3$. We write $(\boldsymbol{\alpha}^1, \Psi_1, \boldsymbol{\alpha}^2, \Psi_2, \boldsymbol{\alpha}^3, \Psi_3) = F(\boldsymbol{\theta})$ and prove that $F$ is locally invertible near $\mathcal{M}$. On $\mathcal{M}$, we have

$$
\left. \frac{\partial \alpha_{j(k,l)}}{\partial \theta_m} \right|_{\mathcal{M}} = \begin{cases} -i & \text{if } m \neq j_{(k,l)}, \\ (N_k - 1)i & \text{if } m = j_{(k,l)}, \\ 0 & \text{otherwise}, \end{cases}
$$

$$
\left. \frac{\partial \Psi_k}{\partial \theta_m} \right|_{\mathcal{M}} = \begin{cases} \frac{1}{N_k} & \text{if } m \in \mathcal{N}_k, \\ 0 & \text{otherwise}. \end{cases}
\tag{A.1}
$$

Using (A.1), the Jacobian of $F$ evaluated on $\mathcal{M}$ can be written as

$$
\left. \frac{dF}{d\boldsymbol{\theta}} \right|_{\mathcal{M}} = \begin{pmatrix} A_1 & \mathbf{0}_{N_1,N_2} & \mathbf{0}_{N_1,N_3} \\ \mathbf{0}_{N_2,N_1} & A_2 & \mathbf{0}_{N_2,N_3} \\ \mathbf{0}_{N_3,N_1} & \mathbf{0}_{N_3,N_2} & A_3 \end{pmatrix},
$$

where

$$
A_k = \begin{pmatrix} (N_k - 1)i & -i & \cdots & & \cdots & -i \\ -i & \ddots & \ddots & & -i & \vdots \\ \vdots & & \ddots & \ddots & & \vdots \\ -i & \cdots & -i & (N_k - 1)i & & -i \\ \frac{1}{N_k} & \cdots & \cdots & & \cdots & \frac{1}{N_k} \end{pmatrix} \in \mathbb{R}^{N_k \times N_k}.
$$

Each $A_k$, and hence $\frac{dF}{d\boldsymbol{\theta}}|_{\mathcal{M}}$ is invertible with

$$
A_k^{-1} = \begin{pmatrix} -\frac{i}{N_k} & 0 & \cdots & 0 & 1 \\ 0 & \ddots & \ddots & \vdots & \vdots \\ \vdots & \ddots & \ddots & 0 & \vdots \\ 0 & \cdots & 0 & -\frac{i}{N_k} & \vdots \\ \frac{i}{N_k} & \cdots & \cdots & \frac{i}{N_k} & 1 \end{pmatrix} \in \mathbb{R}^{N_k \times N_k}.
\tag{A.2}
$$

This concludes the proof that $F : \boldsymbol{\theta} \mapsto (\boldsymbol{\alpha}^1, \Psi_1, \boldsymbol{\alpha}^2, \Psi_2, \boldsymbol{\alpha}^3, \Psi_3)$ is locally invertible in a neighborhood of $\mathcal{M}$. Hence, the change of variables from $\boldsymbol{\theta} \mapsto (\boldsymbol{\alpha}^1, \Psi_1, \boldsymbol{\alpha}^2, \Psi_2, \boldsymbol{\alpha}^3, \Psi_3)$ is well defined near $\mathcal{M}$.

## Appendix B: Proof of the Attractivity of the Slow Manifold

In this appendix, we show that $\mathcal{M}$, the invariant manifold of (1) defined by $\theta_j = \Psi_k$, $j \in \mathcal{N}_k$, $k = 1, 2, 3$, is attractive. This is done by proving for the boundary layer

dynamics

$$\frac{d\alpha_j}{dt} = g_j\big(\boldsymbol{\alpha}^1, \boldsymbol{\alpha}^2, \boldsymbol{\alpha}^3, \Psi_1, \Psi_2, \Psi_3, 0\big), \quad j \in \mathcal{N}_k, \ j \neq j_{(k,N_k)}, \ k = 1, 2, 3,$$

local exponential stability uniformly in $\Psi_1, \Psi_2, \Psi_3$ of the invariant manifold $\mathcal{M}$.

The boundary layer dynamics can be written as

$$\dot{\alpha}_j = i N_1 \alpha_j \bigg( -\frac{N_1}{N}\rho_1 \sin(\Psi_1 - \theta_j) + \frac{N_2}{N}\rho_2\big(\sin(\Psi_2 - \theta_j) - \rho_1 \sin(\Psi_2 - \Psi_1)\big)$$

$$+ \frac{N_3}{N}\rho_3\big(\sin(\Psi_3 - \theta_j) - \rho_1 \sin(\Psi_3 - \Psi_1)\big)\bigg), \quad j \in \mathcal{N}_1, \ j \neq j_{(1,N_1)},$$

$$\dot{\alpha}_j = i N_2 \alpha_j \bigg( -\frac{N_2}{N}\rho_2 \sin(\Psi_2 - \theta_j) + \frac{N_1}{N}\rho_1\big(\sin(\Psi_1 - \theta_j) - \rho_2 \sin(\Psi_1 - \Psi_2)\big)$$

$$+ \frac{N_3}{N}\rho_3\big(\sin(\Psi_3 - \theta_j) - \rho_2 \sin(\Psi_3 - \Psi_2)\big)\bigg), \quad j \in \mathcal{N}_2, \ j \neq j_{(2,N_2)},$$

$$\dot{\alpha}_j = i N_3 \alpha_j \bigg( -\frac{N_3}{N}\rho_3 \sin(\Psi_3 - \theta_j) + \frac{N_1}{N}\rho_1\big(\sin(\Psi_1 - \theta_j) - \rho_3 \sin(\Psi_1 - \Psi_3)\big)$$

$$+ \frac{N_2}{N}\rho_2\big(\sin(\Psi_2 - \theta_j) - \rho_3 \sin(\Psi_2 - \Psi_3)\big)\bigg), \quad j \in \mathcal{N}_3, \ j \neq j_{(3,N_3)}.$$

The linearization of the boundary layer model is given by

$$\frac{\partial \dot{\alpha}_j}{\partial \alpha_m}\bigg|_{\mathcal{M}} = -i\frac{N_k}{N}\left( \frac{\partial \theta_j}{\partial \alpha_m}\bigg|_{\mathcal{M}} \bigg(N_k + \sum_{l \neq k} N_l \cos(\Psi_l - \Psi_k)\bigg) \right.$$

$$\left. + \frac{\partial \rho_k}{\partial \alpha_m}\bigg|_{\mathcal{M}} \sum_{l \neq k} N_l \sin(\Psi_l - \Psi_k) \right),$$

$$j \in \mathcal{N}_k, \ j \neq j_{(k,N_k)}, \ k = 1, 2, 3, \ m \in \{1, \ldots, N\} \setminus \{j_{(1,N_1)}, j_{(2,N_2)}, j_{(3,N_3)}\}. \quad \text{(B.1)}$$

Using (A.2), the values for $\frac{\partial \theta_j}{\partial \alpha_m}|_{\mathcal{M}}$ can be read as

$$\frac{\partial \theta_j}{\partial \alpha_m}\bigg|_{\mathcal{M}} = \begin{cases} -\frac{i}{N_k} & \text{if } m = j, \\ 0 & \text{otherwise.} \end{cases} \quad \text{(B.2)}$$

Taking partial derivatives with respect to $\alpha_m$ of (2) yields

$$\frac{\partial \rho_k}{\partial \alpha_m} e^{i\Psi_k} + \rho_k i \frac{\partial \Psi_k}{\partial \alpha_m} e^{i\Psi_k} = \frac{i}{N_k} \sum_{j \in \mathcal{N}_k} \frac{\partial \theta_j}{\partial \alpha_m} e^{i\theta_j}. \quad \text{(B.3)}$$

Evaluating (B.3) on $\mathcal{M}$ and using (A.2) gives

$$\frac{\partial \rho_k}{\partial \alpha_m}\bigg|_{\mathcal{M}} = \frac{i}{N_k} \sum_{j} \frac{\partial \theta_j}{\partial \alpha_m}\bigg|_{\mathcal{M}} = 0. \quad \text{(B.4)}$$

Plugging (B.2) and (B.4) into (B.1), the Jacobian can be rewritten as a diagonal matrix $J$ with

$$J_{jj} = -\frac{1}{N}\left(N_k + \sum_{l \neq k} N_l \cos(\Psi_l - \Psi_k)\right), \quad j \in \mathcal{N}_k, \ j \neq j_{(k,N_k)}, \ k = 1, 2, 3.$$

When $N_1 = N_2$ and $N_3 = 0$, this matrix has all its eigenvalues strictly negative. This concludes the proof that the boundary layer dynamics are locally exponentially stable uniformly in $\Psi_1, \Psi_2, \Psi_3$ at the invariant manifold $\mathcal{M}$. Hence, $\mathcal{M}$ the invariant manifold of (1) defined by $\theta_j = \Psi_k$, $j \in \mathcal{N}_k$, $k = 1, 2, 3$, is attractive.

## References

Biyik, E., Arcak, M.: Area aggregation and time scale modeling for sparse nonlinear networks. In: Proceedings of the 45th IEEE Conference on Decision and Control, pp. 4046–4051 (2006)

Cardy, J.L., Ostlund, S.: Random symmetry-breaking fields and the XY model. Phys. Rev. B **25**, 6899–6909 (1982)

Couzin, I.D., Krause, J.: Self-organization and collective behaviour in vertebrates. Adv. Study Behav. **32**, 1–75 (2003)

Couzin, I.D., Krause, J., Franks, N.R., Levin, S.A.: Effective leadership and decision making in animal groups on the move. Nature **434**, 513–516 (2005)

Guckenheimer, J., Holmes, P.: Nonlinear Oscillations, Dynamical Systems, and Bifurcations of Vector Fields. Springer, New York (1983)

Justh, E., Krishnaprasad, P.S.: Equilibria and steering laws for planar formations. Syst. Control Lett. **52**(1), 25–38 (2004)

Khalil, H.K.: Nonlinear Systems, 3rd edn. Prentice Hall, New York (2002)

Krause, J., Ruxton, G.D.: Living in Groups. Oxford University Press, Oxford (2002)

Kuramoto, Y.: Chemical Oscillations, Waves, and Turbulence. Springer, Berlin (1984)

Leonard, N.E., Paley, D., Lekien, F., Sepulchre, R., Fratantoni, D., Davis, R.: Collective motion, sensor networks and ocean sampling. Proc. IEEE **95**(1), 48–74 (2007)

Lindauer, M.: Communication in swarm-bees searching for a new home. Nature **179**, 63–67 (1957)

Mauboussin, M.J.: More than You Know: Finding Wisdom in Unconventional Places. Columbia University Press, New York (2006)

Mirollo, R.E., Strogatz, S.H.: Jump bifurcation and hysteresis in an infinite-dimensional dynamical system of coupled spins. SIAM J. Appl. Math. **50**(1), 108–124 (1990)

Moon, S.J., Nabet, B., Leonard, N.E., Levin, S.A., Kevrekidis, I.G.: Heterogeneous animal group models and their group-level alignment dynamics; an equation-free approach. J. Theor. Biol. **246**, 100–112 (2007)

Poston, T., Stewart, I.: Catastrophe Theory and Its Applications. Pitman, London (1978)

Sepulchre, R., Paley, D., Leonard, N.E.: Stabilization of planar collective motion: all-to-all communication. IEEE Trans. Autom. Control **52**(5), 811–824 (2007)

Sepulchre, R., Paley, D., Leonard, N.E.: Stabilization of planar collective motion with limited communication. IEEE Trans. Autom. Control **53**(3), 706–719 (2008)

Strogatz, S.: Nonlinear Dynamics and Chaos. Perseus (1994)

Strogatz, S.H.: From Kuramoto to Crawford: exploring the onset of synchronization in populations of coupled oscillators. Physica D **143**, 1–20 (2000)

Thom, R.: Structural Stability and Morphogenesis. Benjamin, New York (1972)